Analysis of Solid-State Saturable Absorbers and Their Application to Passive Q switching of Lasers

by

Huseyin Cankaya

A Thesis Submitted to the
Graduate School of Engineering
in Partial Fulfillment of the Requirements for
the Degree of

Master of Science
in
Materials Science and Engineering

Koc University

August 2006

Koc University

Graduate School of Sciences and Engineering

This is to certify that I have examined this copy of a master's thesis by

Huseyin Cankaya

and have found that it is complete and satisfactory in all respects,
and that any and all revisions required by the final
examining committee have been made.

Committee Members:

_____

Alphan Sennaroğlu, Ph.D. (Advisor)

_____

Alper Kiraz, Ph. D.

_____

Alkan Kabakçıoğlu, Ph. D.

Date: _____

ÖZET

Cr^{4+}:YAG ve Cr^{2+}:ZnSe kristalleri, sırasıyla 1000 ve 1500 nm civarında çalışan laserlerin pasif Q anahtarlanmasında kullanılabilen katıhal doyabilen soğuruculardır. Bu tezin ilk bölümünde, Cr^{2+}:ZnSe kristalinin doyabilen soğurma özelliklerini incelemek için deneysel ve sayısal teknikler kullandık. Özellikle, Cr^{2+}:ZnSe kristalinin kayıp miktarını, yaşam süresini, temel düzey ve uyarılmış düzey soğurma arakesitlerini 1570 ve 1800 nm dalga boylarında ölçtük. Elde edilen değerler, daha önce literatürde yayınlanan sonuçlarla karşılaştırıldı. Tezin ikinci bölümünde, Cr^{4+}:YAG katıhal doyabilen soğurucusunun Nd:YVO_4 ve Nd:YAG laserlerinin Q anahtarlamasındaki kullanımını inceledik. Bu çalışmada, 1064 nm dalga boyunda ve nanosaniye süreli laser darbeleri elde ettik. Ayrıca Q anahtarlamalı Nd:YVO_4 laserinin darbe tekrar sıklığını ayarlamak için yeni bir yöntem geliştirdik. Bu yöntemde, laser kovuğu içerisinde hareket edebilir bir mercek sayesinde, laser ve pompa ışın demetlerinin çakışmasını değiştirerek laserin optik kazancını ve dolayısıyla darbe tekrar sıklığını kontrol edebildik. Son olarak, Nd:YVO_4 kristalinin 1064 nm'deki ışıma arakesitini, darbe tekrar sıklığı ölçümlerini kullanarak belirledik.

ABSTRACT

Cr^{4+}:YAG and Cr^{2+}:ZnSe are solid-state saturable absorbers which can be used for passive Q switching of lasers operating near 1000 and 1500 nm, respectively. In the first part of the thesis, we employed experimental and numerical techniques to analyze the saturation characteristics of Cr^{2+}:ZnSe. In particular, ground-state and excited-state absorption cross sections, single-pass-loss, and lifetime of the Cr^{2+}: ZnSe saturable absorber were determined at the wavelengths of 1570 and 1800 nm. The results were compared with previously reported values in the literature. In the second part of the thesis, the application of the Cr^{4+}:YAG saturable absorbers in the passive Q switching of Nd:YVO_4 and a Nd:YAG lasers was experimentally investigated. This resulted in the generation of nanosecond laser pulses at the wavelength of 1064nm. In the particular case of the Nd:YVO_4 laser, we developed a technique to adjust and control the pulse repetition rate of the passively Q-switched laser with an intracavity lens. Experimental data showing the performance as a function of the pump power and resonator configuration were obtained. Finally, the emission cross section of Nd:YVO_4 crystal at 1064 nm was determined from the repetition rate data.

ACKNOWLEDGEMENTS

This thesis will be on “Analysis of solid-state saturable absorbers and their applications to passive Q switching”. As my work for a MS degree at Koc University ends, I would like to thank all the people that have provided me technical, economical and non-technical support.

First and foremost, I would like to thank my thesis advisor Prof. Alphan Sennaroglu for all the guidance and technical support during these years. I would also like to thank Adnan Kurt for his constant involvement with my research at KU and his personal support. My interaction with Prof. Sennaroglu and Adnan Kurt has provided me a great opportunity to gain not only experience in experimental research but also non-technical skills.

Umit Demirbas has also contributed significantly to this project and I would like to thank for their continuing support during this work. It was impossible to complete this work in this period. During these years, I have enjoyed interacting with the student members of KU LRL group. I especially would like to thank Hamit Kalaycioglu for his continuing support during the last two years.

I would also like to thank Dr. Alper Kiraz and Dr. Alkan Kabakcioglu for taking their valuable time to serve on my thesis committee.

The primary support for my studies was provided by KU and TÜBITAK. I am grateful for their support without which this work would not have been possible.

Finally, I wish to thank my family and Zeynep Basli for their continuing support, love and patience during my entire time at KU.

TABLE OF CONTENTS

LIST OF TABLES

LIST OF FIGURES

NOMENCLATURE

ν_p	pump photon frequency
ν_l	laser photon frequency
I_p	pump photon intensity
I_l	laser photon intensity
P_p	pump power
P_l	laser power
ϕ_p	normalized transverse intensity distribution for the pump beam
ϕ_l	normalized transverse intensity distribution for the laser beam
ω_p	spotsize function for the pump beam
$\overline{E}_p$	integrated pump pulse energy per unit area
A	cross sectional area
u_p	electromagnetic energy density at the pump wavelength
u_l	electromagnetic energy density at the laser wavelength
v_g	group velocity of the electromagnetic wave
h	Planck's constant
$\|g\rangle$	ground-state energy level
$\|1\rangle$	first state energy level
$\|2\rangle$	second state energy level

$\|3\rangle$	upper energy level
$\|4\rangle$	higher energy level
N_g	ion population density in the ground-state
N_1	ion population density in the first state
N_2	ion population density in the second state
N_3	ion population density in upper energy level
N_4	ion population density in higher energy level
N_t	total active ion population density
σ_e	stimulated emission cross section
σ_a	ground-state absorption cross section
σ_{esa}	excited-state absorption cross section at the pump wavelength
$(\sigma_{esa})_l$	excited-state absorption cross section at the laser wavelength
f_p	normalized excited-state absorption cross section at the pump wavelength
f_l	normalized excited-state absorption cross section at the laser wavelength
f_{rep}	repetition frequency of Q-switched laser
P_{av}	average laser output power
E_p	laser output pulse energy
$\left(P_p\right)_{th}$	threshold pump power
η_s	slope efficiency of the laser
η_p	pumping efficiency
E_{st}	stored energy in the laser cavity

L_g	length of the gain medium
l_{out}	output coupling coefficient
τ_f	fluorescence lifetime of the upper energy level
I_{sa}	absorption saturation intensity
E_{sa}	absorption saturation energy
I_{se}	saturation intensity of emission
α_{p0}	small-signal differential absorption coefficient at the pump wavelength
g_0	small-signal gain coefficient
g	single-pass power gain
g_i	initial single-pass power gain
g_f	final single-pass power gain
Δg	gain reduction
q	single-pass saturable loss coefficient
q_0	initial single-pass saturable loss coefficient
l	total non-saturable loss coefficient of the cavity
τ_l	fluoresce lifetime of the upper laser level of the gain medium
E_L	absorption saturation energy of the gain medium
E_A	absorption saturation energy of the saturable absorber
I_l^+	laser photon intensity propagating in $+z$ direction
I_l^-	laser photon intensity propagating in $-z$ direction
P_{pi}	incident pump power
T_R	cavity round-trip time

Chapter 1

INTRODUCTION

Q switching is a widely used technique for obtaining pulsed laser output with high peak power. In this technique, the quality factor of the laser cavity is controlled by an optical switch. When the quality factor is high, the average lifetime of the photons circulating inside the cavity is long. In other words, the quality factor shows the degree of loss inside the cavity. When the quality factor is low, the laser cannot operate but the gain inside the gain medium builds up. If we suddenly increase the quality factor, the gain inside the cavity is depleted by stimulated emission and the power inside the cavity grows quickly from the noise level. As a result of this, a Q-switched pulse is released. Q switching can be achieved by using rotating mirrors, electro-optical switches or saturable absorbers. In the case of the "rotating mirror" technique, one of the cavity end mirrors is rotated about an axis perpendicular to the cavity axis. By this way, the loss of the cavity is very high except when the mirrors are parallel to each other. In electro-optical Q-switching, the quality factor is controlled by using an electro-optical shutter placed inside the cavity. Two of the most commonly used electro-optical shutters are Pockels cell and frustrated total internal reflection prism (FTIR). The electro-optical shutters can be controlled by applying a high voltage on the shutter. Because, the shutter and hence the repetition rate of the Q-switched pulses are externally controlled, these are classified as active Q switching methods. On the other hand, passive Q switching uses saturable absorbers in which pulse shaping occurs with no external modulation. In passive Q switching, the saturable absorber acts as a passive optical switch inside the cavity. The transmission of the light incident on the

saturable absorber depends on the incident photon intensity and the saturation parameters of the saturable absorber. When the intensity becomes high, the transmission is increased and hence the shutter 'opens up'. The scope of this thesis is to determine the saturation parameters of the Cr^{2+}:ZnSe saturable absorber and demonstrate the application of Cr^{4+}:YAG saturable absorbers in the passive Q switching of neodymium lasers. The organization of the thesis is as follows: In the second chapter, we will summarize the previously reported studies on the determination of the saturation parameters of the Cr^{2+}:ZnSe and Cr^{4+}:YAG saturable absorbers and their application in passive Q switching. In Chapter 3, we will give the theoretical background needed for the analysis of the saturable absorbers and passive Q switching. In Chapter 4, we will focus on the determination of the saturation parameters of the Cr^{2+}:ZnSe saturable absorber. First, we will describe the experimental setup. Then, we will show the experimental results and explain the analysis procedure. Finally, we will discuss the results and compare with the previously reported values. In Chapter 5, we discuss the operation of passively Q-switched Nd:YVO_4 and Nd:YAG lasers operating at 1064 nm. Cr^{4+}:YAG saturable absorbers were used to initiate passive Q switching. In the particular case of the Nd:YVO_4 laser, an intracavity lens was used to develop a scheme for adjusting and controlling the pulse repetition rate application. In the case of the Nd:YAG laser, output pulse energies up to 80 mJ could be obtained at a repetition rate of 1 Hz. For both cases, the output pulsewidths were in the 40-100 ns range.

Chapter 2

LITERATURE REVIEW

2.1 Overview

Pulsed solid state lasers operating in the near and mid infrared spectral region (0.8-2.5μm) are widely used in telecommunications, range finding, and medical applications. In that spectral region, Cr^{4+}:YAG and Cr^{2+}:ZnSe are very attractive solid-state laser gain media in terms of stability under thermal loading, large emission cross section, pump source availability and broad tunability. Many researchers investigated laser characteristics of these materials [1-4]. In addition, these materials can be used in passive Q switching of solid state lasers to produce pulsed laser output in the nanosecond time scales. In passive Q switching applications, the ground-state absorption cross section (σ_a) and excited-state absorption cross section (σ_{esa}) are important parameters determining the saturation intensity of the crystals. Many groups used different techniques to determine these parameters and they also demonstrated passive Q switching of various solid state lasers. In this chapter, we summarize previous studies done on the determination of saturation characteristics of Cr^{4+}:YAG and Cr^{2+}:ZnSe crystals and their application in passive Q switching.

2.2 Cr^{4+}:YAG Saturable Absorbers

In previous studies, the ground-state absorption cross section of Cr^{4+}:YAG was determined by two experimental methods. In the first method, transmission of a saturable absorber is measured by varying the incident pump power. In the second method (also referred as the z-scan method), the transmission is measured at constant pump power but the photon

intensity inside the saturable absorber is varied by changing the spot size inside the sample. In this section, the investigations of the saturation characteristics of Cr^{4+}:YAG and its application in passive Q switching of Nd:YAG and Nd^{3+}:YVO_4 lasers at 1064 nm reported in previous studies will be presented. The ground-state and normalized excited-state absorption cross section f_p ($f_p = \sigma_{esa}/\sigma_a$) values reported in the literature are summarized in Table 2.1:

σ_a ***(x10^{-18} cm^2)***	f_p	***References***
5.7	0.14	[5]
4.48	<0.004	[6]
7	0.29	[7]
1.64	0.28	[8]
0.55	-	[9]
3.2	0.14	[10]
3	0.07	[11]
1.96	0.06	[12]
1.4	0.09	[4]
3.21	<0.13	**Average**

Table 2.1: Ground-state and normalized excited-state absorption cross section values of Cr^{4+}:YAG reported in the literature.

The ground-state absorption cross section of Cr^{4+}:YAG depends on the crystal orientation even though YAG crystal is centrosymmetric [13] because of the orientation of the dipole moment of resonantly absorbing transition. Eiler et al. [5] determined the saturation parameters for the case when the laser light was propagating along both the [001] and [111] crystallographic axes of Cr^{4+}:YAG. In the experiments, a pulsed laser operating at 1064 nm with 10 ns pulsewidth was used. The samples were rotated about these crystal axes during the experiment to reveal the dependence of the transmission on rotation of the crystals. The experimental results showed that Cr^{4+}:YAG crystal was highly anisotropic in the saturation regime. The dipole moment of the energy transition from ground to the excited state were assumed to be aligned along one of the crystallographic

axes [100], [010] or [001]. The modeling of the saturation phenomenon along specified crystallographic axes was carried out by a set of rate equations. The highest ground and excited-state absorption cross sections at 1.064 μm were found to be 5.7 x 10^{-18} cm^2 and 0.8 x 10^{-18} cm^2, respectively.

Miller and co-workers [14] analyzed the saturation characteristics of Cr^{+4}:YAG saturable absorber in two steps and demonstrated the application in passive Q switching of diode-pumped Nd:YAG laser. In the first step of the analysis, the transmission of the Cr^{+4}:YAG crystal was shown with respect to incident pump intensity. In the second step, temporal recovery of Cr^{4+} saturation was studied by a pump-probe experiment. In passive Q switching experiments, the output coupling was varied and the pump photon intensity on the saturable absorber was changed by translating the lens inside the cavity to optimize the pulse energy. As high as 12 mJ of energy per pulse was obtained.

Spariosu et al. reported [11] the dual operation of Cr^{4+}:YAG as a laser active material and a passive optic switch inside an optical resonator for the first time. In this study, Cr^{4+}:YAG crystal was pumped by a flash-lamp-pumped Nd:YAG laser and the pulses with 35 and 100 ns pulse durations were obtained at 1.06 and 1.44 μm, respectively. The repetition rate of the pulses was 30 kHz. The ground-state and excited-state absorption cross sections of the Cr^{4+}:YAG crystal were determined to be $3x10^{-18}$ and $2x10^{-19}$ cm^2,respectively, by bleaching the samples.

Yankov [15] demonstrated passive Q switching of flash-lamp-pumped Nd-doped lasers, namely Nd:YAG, Nd:$YAlO_3$, and Nd:KGW lasers. Q switching was achieved by a using Cr^{+4}:YAG crystal inside the laser cavity. In bleaching experiments, the double-pass transmission of the Cr^{+4}:YAG crystal was measured since one surface of the Cr^{+4}:YAG sample was highly reflective at 1064 nm. The depolarization of the transmitted laser beam was determined by rotating the saturable absorber around the optical axis. During the

operation of Nd:YAG, Nd:$YAlO_3$, Nd:KGW lasers at 10 Hz, Q-switched pulses with output energies of 26, 52 and 16 mJ were obtained, respectively.

Shimony and co-workers [16] investigated the absorption saturation parameters of Cr^{4+}:YAG saturable absorber and demonstrated passive Q switching of a flash-lamp-pumped Nd:YAG laser. The Cr^{4+}:YAG crystal has a dual function inside the laser cavity as passive optic switch and as a Brewster plate to obtain polarized laser light. The stepped efficiency curve of the Q-switched laser was addressed as shown in Figure 2.1(c) and it was attributed to the insufficient energy for laser operation after occurrence of the first output pulse.

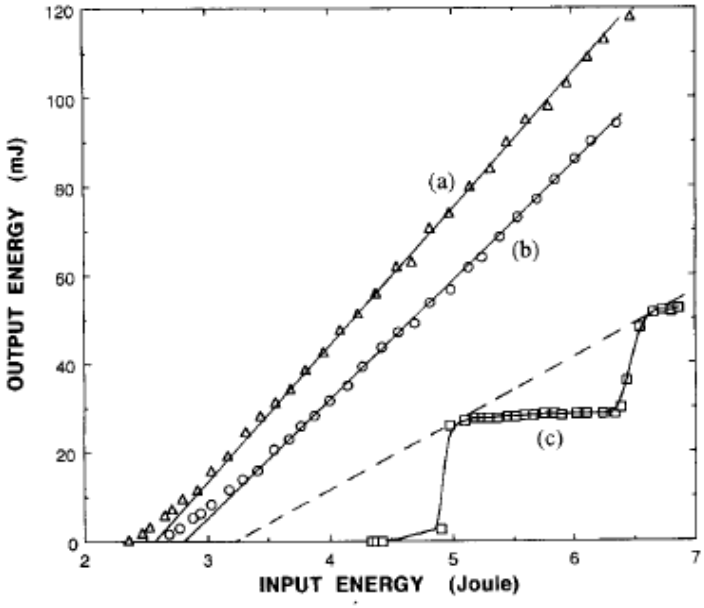

Figure 2.1: Output vs. input pump energy of a Nd:YAG laser under free-running (a) and (b), and passively Q-switched (c) conditions. Curve (b) was measured with undoped YAG as a Brewster plate [16].

In this work, the ground-state and excited-state absorption cross sections of Cr^{4+}:YAG were determined by bleaching the samples. In bleaching experiments, a Q-switched Nd:YAG laser was used as the pump source at 1064 nm. In the analysis, the ground-state

and excited-state absorption cross sections were determined to be 8.7×10^{-19} and 2.2×10^{-19} cm^2, respectively. The analysis was carried out by using a simple transmission relation which ignores Gaussian distribution of the pump laser. However in their later work [7], the ground-state and excited-state absorption cross sections were re-estimated to be 7×10^{-18} and 2×10^{-18} cm^2, respectively by using a modified Frantz-Nodvik Equation. The original Frantz-Nodvik Equation is a solution of the rate equations for a four-level energy system when the excited-state absorption is negligible and the pump beam is uniform inside the saturable absorber. However the excited-state absorption can not be neglected for the Cr^{4+}:YAG saturable absorber and the pump beam is not generally uniform inside the crystal. In order to solve this problem, Frantz-Nodvik Equation was modified by taking into account these conditions and an expression was derived for the transmission (T) of the saturable absorber in the low-energy limit as follows:

$$T = T_0\left(1 + \frac{\sigma_a - \sigma_{esa}}{2}(1 - T_0)E\right) \quad \text{for} \quad (\sigma_a - \sigma_{esa})E < 1. \qquad (2.2.1)$$

Here, E is half of the Gaussian peak energy density of the pump and T_0 is the small-signal limit of energy transmission in the saturable absorber. In this work, the researchers also determined the absorption cross sections of other Cr^{4+} garnets, namely Cr^{4+}:GGG and Cr^{4+}:YSGG and compared them with each other. The excited-state absorption spectrum of the samples between 700 and 900 nm was measured under Ti:sapphire laser excitation.

In another study, the same group experimentally investigated the performance of Cr^{4+}:YAG crystal at 1064 nm as passive Q-switch inside a flash-lamp-pumped Nd:YAG laser cavity [17]. The Cr^{4+}:YAG samples were cut parallel to the [111] crystallographic axis. In this study, it was proposed that the pulsewidth of the laser output could be varied by adjusting the losses inside the cavity. The losses could be varied by changing either the thickness of the saturable absorber, or its doping level. In Q switching experiments, as high as 200 mJ of pulse energy was obtained and the output pulse duration was 28 ns. In a later

study of the same group [18], passive Q switching of continuous-wave Nd:YAG laser with Cr^{4+}:YAG laser was demonstrated for the first time. The pulse repetition rate and pulse duration varied in the range of 2-29 kHz and 80-300 ns, respectively, depending on the small-signal absorption coefficient of the saturable absorber and pump power. The correlation between repetition rate and the output power was modeled by using Powell and Wolga's rate equation approach on passive Q switching of continuous-wave lasers [19]. In these rate equations, the contribution of spontaneous emission to the photon density is neglected and all the densities are assumed to be homogeneously distributed inside the laser cavity. Powell and Wolga suggested an approximate expression for the repetition frequency (f_{rep}) of Q-switched laser as follows:

$$f_{rep}{}^2 \approx \frac{(1+c\sigma_e\tau_a S_{av})(1+c\sigma_a\tau_s S_{av})}{\tau_s\tau_a} + \left[\frac{c\sigma_e n_{ao}}{\tau_a + \dfrac{1}{c\sigma_e S_{av}}} - \frac{c\sigma_a n_{so}}{\tau_s + \dfrac{1}{c\sigma_a S_{av}}}\right]. \qquad (2.2.2)$$

Above, σ_e is the emission cross section of the gain medium, τ_a and τ_s are the excited-state lifetime of gain medium and saturable absorber, respectively, c is the speed of light, S_{av} is average photon density inside the cavity, n_{a0} is the laser excited-state density and n_{s0} is the ground-state density of the saturable absorber.

Sennaroglu investigated the saturation characteristics of Cr^{4+}:YAG by accounting for thermal loading [9]. In this study, the experiments were carried out in two parts: In the first part, the fluorescence lifetime of the Cr^{4+}:YAG saturable absorber was measured by using a Q-switched Nd:YAG laser in the 5-50°C temperature range. In the second part, continuous-wave transmission of the saturable absorber at 1064 nm was measured by varying the crystal boundary temperature. A model was developed to describe the saturation phenomenon. The model takes into account the spatial distribution of the pump beam, the temperature dependence of refractive index and the fluorescence lifetime of the saturable

absorber. In the calculations, first the temperature distribution with constant saturation intensity was calculated. Second, the beam propagation parameters were modified according to the temperature distribution inside the crystal. As a result of the analysis, the ground-state absorption cross section was determined to be $5.5x10^{-19}cm^2$.

Kalisky and co-workers compared the saturation parameters of Cr^{4+}-doped YAG, YSGG and LuAG, and demonstrated the application in passive Q switching at 1064 nm [10]. The samples were bleached by a pulsed Nd:YAG laser (350mJ pulse energy, 8-45 ns pulsewidth) to measure the ground-state and excited-state absorption cross sections of the crystals. In the analysis, a modified Frantz-Nodvik Equation, which takes into account the excited state absorption, was used to model the saturation phenomena. The ground-state and excited-state absorption cross sections were determined to be $3.2x10^{-18}$ cm^2 and $4.5x10^{-19}$ cm^2, respectively. As an application, passively Q-switched Nd:YAG laser with 52 ns pulsewidth was demonstrated. The peak power of the Q-switched pulses was 10 times higher than the free running peak power of the Nd:YAG laser.

As an alternative method, Xiao et al. [8] used z-scan measurements to determine the ground-state and excited-state absorption cross sections of Cr^{+4}:YAG at 1064 nm and discussed the effect of the absolute value of the cross sections in passive Q switching. In this study, a rate equation analysis for a 4-level energy system, which takes into account the spatial distribution of the pump beam, was employed in the determination of absorption cross sections. The z-scan measurements were carried out by using a Q-switched mode-locked Nd:YAG laser. The z-scan measurement was conducted with very low incident pulse energy (0.27 μJ) to determine the ground-state absorption cross section. The fitting of the experimental data with the theoretical model was carried out by changing only the ground-state absorption cross section since the excited-state absorption became significant at high incident energy and there could be many combinations of two cross sections that fit the experimental data for a single z-scan measurement. From the fittings, the average

ground-state absorption cross section of the crystals produced by different sources was found to be 1.64×10^{-18} cm^2 at 1064 nm. By using the measured ground-state absorption cross sections, the average excited-state absorption coefficient were determined to be 0.46×10^{-18} cm^2. The z-scan measurements were also conducted at the temperature range from -60˚C to 90˚C and it was concluded that the ground and excited-state absorption cross sections were independent of temperature. Xiao also demonstrated that the absolute values of the cross sections had no effect on the output energy of passively Q-switched lasers when the ratio of the ground-state absorption cross section to the product of emission cross section and inversion reduction factor (γ) is much greater than 1 ($\sigma_a / (\sigma_e \gamma) > 1$).

Okchrimchuck and co-workers [6] explained the relationship between spectroscopic structure and saturation parameters of Cr^{4+}:YAG crystals. A spectroscopic model of Cr^{4+} centers in YAG crystals was proposed to describe the anisotropy of the crystal. In the analysis, a rate equation approach was used to investigate the ground and excited-state absorption cross sections. The saturation of Cr^{4+}:YAG crystals at 1064 nm was described by two ground-state absorption cross sections namely $\sigma_{0\pi}$ and $\sigma_{0\sigma}$ when the electric field incident on the crystal was parallel ($\sigma_{0\pi}$) and perpendicular ($\sigma_{0\sigma}$) to [100] crystallographic axis. The bleaching experiments were conducted by using polarized continuous-wave and pulsed-wave laser light at 1064 nm. $\sigma_{0\pi}$ and $\sigma_{0\sigma}$ were determined to be in the range of $3.9\text{-}5 \times 10^{-18}$ and $1.5\text{-}1.9 \times 10^{-19}$ cm^2, respectively. The excited-state absorption cross section was found to be less than 2×10^{-20} cm^2. The researchers also concluded that the transition between ${}^3B_1({}^3A_2)$ and ${}^3A_2({}^3T_1)$ energy levels was responsible for the absorption band centered at 1000 nm as shown in the energy diagram below:

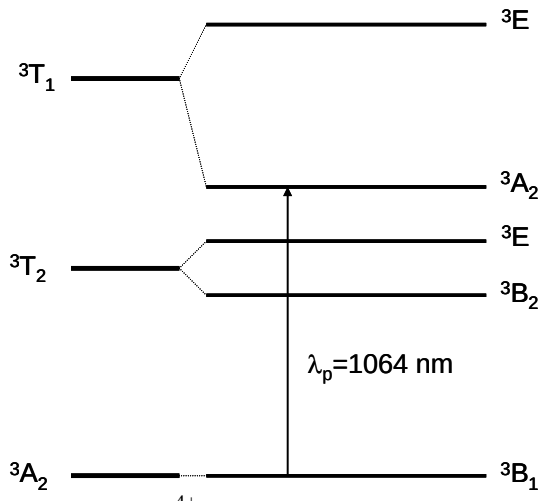

Figure 2.2: Energy diagram of Cr^{4+}:YAG showing the ground-state absorption [6].

Wacihman et al. [20] investigated the cw and pulsed operation of diode side-pumped Nd:YAG and Nd:YVO_4 lasers at 1064 nm. The Q-switched operation was performed by an intracavity Cr^{4+}:YAG saturable absorber. The slope efficiencies in cw operation of Nd:YAG and Nd:YVO_4 lasers were 35 % and 40 %, respectively. In passive Q-switched operation, the slope efficiencies of both lasers decreased but due to relatively low thermal conductivity of Nd:YVO_4 crystal, the efficiency of Nd:YVO_4 laser decreased more dramatically. The highest Q-switched output powers of Nd:YAG and Nd:YVO_4 lasers were 4.2 and 0.8 W, respectively. A decrease in the pulsewidth of the Q-switched pulses was observed when the pump power was increased.

Liu et al. [21] demonstrated an application of Cr^{4+}:YAG saturable absorbers in passive Q switching of diode-end-pumped cw Nd:YVO_4 laser operating at 1064 nm. In this study, cw and pulsed operations of Nd:YVO_4 laser were analyzed with different output couplers and Cr^{4+}:YAG crystals with various amounts of low-power transmission. 4.05 W of cw output power was obtained when the pump power and the transmission of the output coupler were 8 W and 10 %, respectively. In Q-switched operation, the average output power of 1.4 W was achieved with 200 kHz repetition rate and the pulse duration was 60 ns

when a Cr^{4+}:YAG sample with 85 % transmission was used. However, the shortest pulsewidth of 12 ns with highest pulse energy (36 μJ) was obtained when Cr^{4+}:YAG saturable absorber with 85 % transmission was replaced by Cr^{4+}:YAG saturable absorber with 60 %.

Agnesi et al. [22] reported a passively Q-switched high peak-power Nd:YVO_4 laser with output polarized along a-axis. The Q switching operation was performed by using a Cr^{4+}:YAG saturable absorber. In Q-switched operation, 157 μJ pulse energy with 6 ns pulsewidth was obtained and the average output power was 3.6 W. The polarization of the laser was optimized by using the misalignment sensitivity of flat-flat cavity configuration and birefringence of the Nd:YVO_4 active medium.

Sennaroglu and co-workers [12] described an systematic procedure to determine the saturation parameters of Cr^{4+}:YAG and Cr^{4+}:forsterite saturable absorbers at 1064 nm. The bleaching experiments were conducted for two pumping cases: Continuous-wave (cw) and pulsed. In the experiments, a Nd:YAG laser operating at 1064 nm was used as pump source. A rate-equation model was developed to analyze the bleaching experiments for both pumping configurations. The model takes into account the excited-state absorption and spatial distribution of the pump beam inside the saturable absorber. An iterative best-fit algorithm was employed in the analysis of the experimental data. In the determination of saturation parameters, cw and pulsed data were used at the same time as follows: The cw transmission data were first analyzed to find the small-signal absorption coefficient (α_{p0}) of the saturable absorbers. Then pulsed data were used to determine the normalized excited-state absorption cross section (f_p) by fixing α_{p0} to the value obtained from cw analysis. Finally cw transmission data were analyzed by using obtained f_p and α_{p0} to find the ground-state absorption cross section. From the analysis, the average ground-state and normalized excited-state absorption cross sections of Cr^{4+}:YAG were determined to be 19.6×10^{-19} cm^2 and 0.06, respectively.

2.3 Cr^{2+}:ZnSe Saturable Absorbers

Cr^{2+}:ZnSe is an attractive passive optic switch in a wide spectral region (1400-2100 nm). It is generally employed as a saturable absorber to produce pulses in the nanosecond time scale. Nanosecond pulsed lasers are required for range-finding applications, telecommunications, and medical applications in the spectral region where Cr^{2+}:ZnSe can work as passive optical switch. Since the saturation parameters are important in passive Q switching applications, the ground-state and excited-state absorption cross sections of Cr^{2+}:ZnSe were determined by many groups [23-26]. Table 2.2 summarizes the reported ground-state absorption cross section values at different wavelengths in the literature, and the estimated values at 1800 and 1570 nm according to the absorption spectrum of Cr^{2+}:ZnSe:

σ_a ($x10^{-19}cm^2$)	Pump Wavelength (nm)	σ_a at 1800 nm ($x10^{-19}cm^2$)	σ_a at 1570 nm ($x10^{-19}cm^2$)	Reference
11.5	1775	11.3	4.4	[27]
2	2017	7.4	2.9	[23]
4.9	1598	9.8	3.8	[28]
3	2000	9.3	3.6	[25]
3.2	1534	11.7	4.6	[29]
8.7	1775	8.6	3.4	[1]
19	1645	27.5	10.8	[26]
11	1775	10.8	4.2	[30]
Average		12.1	4.7	

Table 2.2: Determined ground-state absorption cross section for Cr^{2+}:ZnSe at different wavelengths and estimated values at 1800 and 1570 nm based on absorption spectrum measurements.

Podlipensky et al. [28] analyzed and compared the saturation characteristics of Cr^{2+}:ZnSe and Co^{2+}:ZnSe. Then, they used these samples as saturable absorbers inside a flash-lamp-pumped Er:glass laser to obtain passively Q-switched pulses at 1540 nm. The saturable absorbers were bleached by a Nd:YAG-pumped $Ba(NO_3)_2$ Raman laser at 1598

nm to determine the saturation parameters experimentally. In the analysis of the experimental data, a modified Avizonis-Grotbeck equation was used as the model. The original Avizonis-Grotbeck Equation describes pump light evolution inside the saturable absorber for a four-level energy system without accounting for excited-state absorption. Kuo and co-workers [31] modified the original equation for the case where the excited-state absorption is significant and they developed the following differential equation:

$$\frac{dF}{dz} = -h\nu N_0\left(1-\frac{\sigma_{esa}}{\sigma_a}\right)\left[1-\exp\left(-\frac{\sigma_a F}{h\nu}\right)\right] - N_0\sigma_{esa}F - \alpha F\,, \qquad (2.3.1)$$

where F is the energy fluence, $h\nu$ is the pump photon energy, N_0 is the total active ion density inside the saturable absorber, and α is the absorption coefficient due to nonsaturable losses. In Podlipensky's work [28], the ground-state absorption cross section of Cr^{2+}:ZnSe was determined to be $4.9\text{x}10^{-19}$ cm^2 at 1598 nm by using the modified equation of Kuo [31]. By the same analysis, the excited-state absorption cross section was estimated to be less than $0.2\text{x}10^{-19}$ cm^2. In passive Q switching of the Er:glass laser by the Cr^{2+}:ZnSe saturable absorber, 5 mJ output pulse energy was obtained with as short as 40-ns pulses. The average Q-switched conversion efficiency was estimated to be % 25.

Tsai et al. [23] demonstrated passive Q switching of Ho:YAG and Tm:YAG lasers by Cr^{2+}:ZnSe saturable absorber at 2090 and 2017 nm, respectively. The output pulse energy of Ho:YAG laser was 1.3 mJ with 90-ns pulse duration and the Q switching efficiency was 5 %. On the other hand, the Q switching efficiency of Tm:YAG laser was 16 % and the pulse energy was 3.2 mJ with 90-ns pulsewidth. The ground and excited-state absorption cross sections of Cr^{2+}:ZnSe were determined by bleaching the samples with passively Q-switched Tm:YAG laser at 2017 nm. The experimental results were modeled by using the modified Avizonis-Grotbeck Equation which accounts for the excited-state absorption and the ground-state absorption cross section was determined to be $2\text{x}10^{-19}$ cm^2 at 2017 nm.

Shcherbitsky and co-workers [29] determined the absorption cross sections of various saturable absorbers (namely Co:ZnS, Co:ZnSe, Cr^{2+}:ZnSe, Co:MALO, Co:LMA) by using the modified Avizonis-Grotbeck model. The modification of Avizonis-Grotbeck Equation is different from other studies explained before because here, the model takes into account both the excited-state absorption and the spatial distribution of the pump beam as expressed below:

$$\frac{dE}{dz} = \alpha E - \frac{\sigma_{esa} E}{l\sigma_a} \ln\left(\frac{1}{T_0}\right) - \frac{\pi\omega^2 F_{sat}}{l} \ln\left(\frac{1}{T_0}\right)\left(1 - \frac{\sigma_{esa}}{\sigma_a}\right)\left(1 - \exp\left(-\frac{E}{\pi\varpi^2 F_{sat}}\right)\right). \quad (2.3.2)$$

In Eq. 2.3.2, E is the pulse energy, l is the length of the saturable absorber, T_0 is the small signal transmission, ω is the beam waist of the pump beam and F_{sat} is the saturation fluence of the saturable absorber. The experiments were carried out by using a flash-lamp-pumped passively Q-switched Er:glass laser with 75-ns pulse duration at 1 Hz. From the analysis, the average ground-state and excited-state absorption cross sections of Cr^{2+}:ZnSe at 1534 nm were determined to be 3.3 $x10^{-19}$ and 0.1$x10^{-19}$ cm^2, respectively.

Qamar et al. [25] demonstrated a passively Q-switched Tm-silica fiber laser at 1900 nm. In this study, the passive Q switching was achieved by using a Cr^{+2}:ZnSe saturable absorber. The Q switching operation was accompanied by self-mode-locking. The saturation parameters of the Cr^{+2}:ZnSe crystal was measured by the bleaching method. In the bleaching experiments, a Tm-silica double-clad fiber laser was employed as the pump source. From the experiments, the ground-state absorption cross section was found to be 3$x10^{-19}$ cm^2 at 2 μm. In laser experiments, the Tm-fiber laser was pumped by Nd:YAG laser operating at 1319 nm. The output pulse of the Tm-fiber laser was optimized by changing the output coupler transmission, fiber length and the pump power. The optimum output coupler reflectivity and fiber length were 4 % and 3.2 mm, respectively, and the optimum peak power of the output pulses with 330 ns pulsewidth was 15 W when the fiber was pumped at 3.6 W.

Stultz et al. [26] reported a passively Q-switched Er:YAG laser operating at 1617 nm with 7-ns pulsewidth and 4 kHz repetition rate. The Q-switched operation was achieved by introducing Cr^{2+}:ZnSe saturable absorber at Brewster angle inside the laser cavity. The Er:YAG laser was pumped by Er:fiber laser operating at 1534 nm. The ground and excited-state absorption cross sections were determined by bleaching the Cr^{2+}:ZnSe sample with 1.2kHz, 78-ns, electro-optically Q-switched Er:YAG laser pulses at 1645 nm. Experimental data were analyzed by using modified Avizonis-Grotbeck equation and the ground-state absorption cross section of the saturable absorber was determined to be $1.9x10^{-18}cm^2$ at 1645 nm. The excited-state absorption cross section was found out to be negligible.

Kisel et al. [32] investigated the luminescence characteristics of single-crystal Cr^{+2}:ZnSe with respect to the concentration and the temperature in the range 77-300 K and they determined the fluorescence lifetime of the upper laser level. The ground and excited-state absorption cross sections at 1534 nm were measured. The bleaching experiments were conducted with a passively Q-switched Er:glass laser producing 75 ns pulses at 1 Hz repetition rate. A four-level model was used in the analysis of saturable absorber and the ground-state absorption cross section was determined to be $3.2x10^{-19}$ cm^2. The excited-state absorption cross section was found to be negligible. Kisel et al also demonstrated the lasing performance of Cr^{+2}:ZnSe single crystal pumped at 1750 nm by eight InGaAs laser diodes and as high as 186 mW of output power was obtained with an efficiency of 31 %.

Chapter 3

MODELLING OF SATURABLE ABSORBERS AND PASSIVE Q SWITCHING

3.1 Introduction

In the analysis of saturable absorbers and passively Q-switched lasers, a standard rate equation analysis will be employed based on a modified 4-level energy system. Such a model accurately describes Cr^{2+}:ZnSe, Cr^{+4}:YAG and Nd:YVO_4 systems. Two different model equations will be derived for the cases of continuous-wave (cw) and pulsed pumping to determine the saturation parameters of the saturable absorbers. The first model describes the pump photon intensity evolution inside the saturable absorber for the cw case. The second model describes the change of the pump pulse energy per unit area for the pulsed case. In the analysis of passive Q switching, a coupled differential equation will be introduced to describe the interaction of the laser power, fractional gain, and saturable loss.

The transitions between the energy levels of a modified 4-level system are shown in Figure 3.1

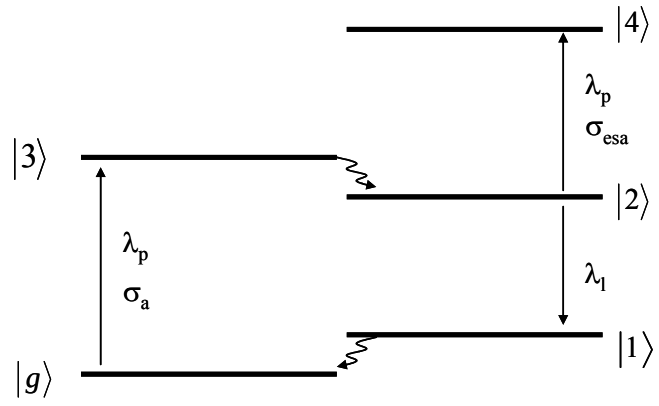

Figure 3.1: Energy-level diagram for a modified 4-level medium with the possibility of excited-state absorption.

When the pump photons with a wavelength of λ_p are absorbed by the ions in the ground-state ($|g\rangle$), they make transition to the upper energy level ($|3\rangle$) and then decay to the second level ($|2\rangle$) very rapidly by non-radiative processes. This process is called "ground-state absorption" and the strength of the absorption depends on the ground-state absorption cross section (σ_a) of the medium. When you increase the photon intensity, the transmission at the pump wavelength increases up to a certain point which is determined by the excited-state absorption and other non-saturable losses of the medium. The increase in the transmission is due to the depletion of the ground-state population at high levels of pumping. This process is called "saturation" or "bleaching" of the medium. The ions in the second level can either absorb the pump photons or decay to the first energy level ($|1\rangle$). In the decay process, the photons with a wavelength of λ_l are emitted by spontaneous or stimulated emission. When the ions in the second level absorb photons with wavelength λ_p, they can also be transferred to a higher level ($|4\rangle$) and this process is called "excited-state absorption". The strength of the excited-state absorption depends on the excited-state absorption cross section (σ_{esa}) of the medium. The interactions described above can be modeled by using the following rate equation:

$$\frac{\partial N_2}{\partial t} = -\frac{\partial N_g}{\partial t} = \frac{I_p \sigma_a N_g}{h\nu_p} - \frac{N_2}{\tau_f} - \frac{I_p \sigma_{esa} N_2}{h\nu_p} - \frac{I_l \sigma_e N_2}{h\nu_l}. \qquad (3.1.1)$$

Above, h is Planck's constant, I_p is the pump photon intensity, I_l is the laser photon intensity, τ_f is fluorescence lifetime of the second energy level, ν_l is the laser photon frequency, ν_p is the pump photon frequency, σ_e is the stimulated emission cross section, N_g is the population density of ions in the ground-state and N_2 is the population density of ions in the second state. The first term at the right hand side of the Eq. 3.1.1 represents

the stimulated absorption of the medium and it is proportional to the pump photon intensity. The second term is due to spontaneous emission from the upper laser level and the third term gives the decay rate due to the excited-state absorption. The fourth is the stimulated emission term and is proportional to the laser intensity at the frequency ν_l. Note that the ion densities in the fourth, third and first levels (N_4, N_3, N_1) are assumed to be negligible because of the fast decaying processes.

3.2 Saturation

In the saturation of absorption, the ground-state and the excited-state absorption cross sections play an important role. In this work, these parameters were determined experimentally for two pumping configurations. During the experiments, the transmission of the pump laser through the saturable absorber is measured with respect to the pump photon intensity incident on the sample. In this section, we will concentrate on modeling of the transmission of the pump laser through the saturable absorber for two pumping configurations: cw and pulsed. In the analysis of saturation, we can neglect the stimulated emission term in Eq. 3.1.1 to obtain

$$\frac{\partial N_2}{\partial t} = -\frac{\partial N_g}{\partial t} = \frac{I_p \sigma_a N_g}{h\nu_p} - \frac{N_2}{\tau_f} - \frac{I_p \sigma_{esa} N_2}{h\nu_p}. \qquad (3.2.1)$$

The total active ion population density (N_t) can be taken as the sum of N_g and N_2 since the excited-state ion populations N_4, N_1 and N_3 are negligible in comparison to N_g and N_2. For the cw case, the time derivatives in Eq. 3.2.1 vanish in steady state, giving the following relation between N_2 and N_t in terms of I_p:

$$N_2 = N_t \frac{\frac{I_p}{I_{sa}}}{1+\frac{I_p}{I_{sa}}}. \tag{3.2.2}$$

Here, I_{sa} is the absorption saturation intensity for the four-level system ($I_{sa} = h\nu_p / \sigma_a \tau_f$). Consider a saturable absorber with a cross sectional area A and an infinitesimal length, dz, as shown in Figure 3.2.

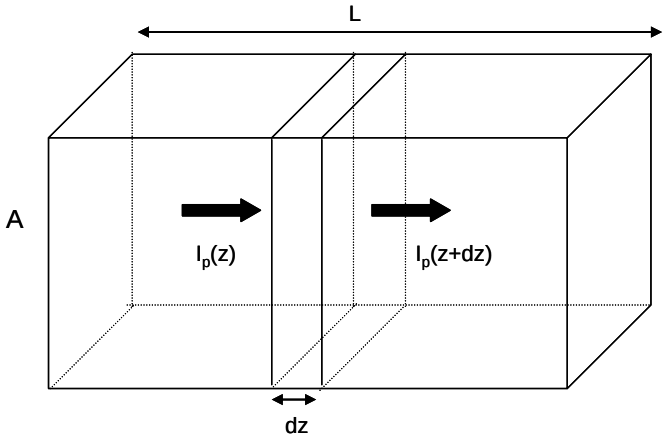

Figure 3.2: Pump beam evolution inside a saturable absorber.

The conservation of energy gives the following relation, where u_p is the electromagnetic energy density at the pump wavelength :

$$Adz\frac{\partial u_p}{\partial t} = \left(I_p(z) - I_p(z+dz)\right)A - \left(N_g\sigma_a I_p + N_2\sigma_{esa} I_p\right)Adz\,. \tag{3.2.3}$$

In Eq. 3.2.3, the loss inside the medium is assumed to be due to the ground-state and excited-state absorption. The expression can be simplified by using the relation $u_p = v_g I_p$ as follows:

$$\frac{\partial I_p}{\partial z} + \frac{1}{v_g}\frac{\partial I_p}{\partial t} = -\sigma_a N_g I_p - \sigma_{esa} N_2 I_p\,. \tag{3.2.4}$$

Here, v_g is the group velocity of the electromagnetic wave. If N_g is expressed in terms of N_2 and N_t in Eq. 3.2.4, the following differential equation is obtained for I_p:

$$\frac{\partial I_p}{\partial z} + \frac{1}{v_g}\frac{\partial I_p}{\partial t} = (1 - f_p)h\nu_p \frac{\partial N_g}{\partial t} - \sigma_{esa} N_t I_p . \tag{3.2.5}$$

In Eq. 3.2.5, f_p is the normalized excited-state absorption cross section at the pump wavelength ($f_p = \sigma_{esa}/\sigma_a$). If we substitute Eq. 3.2.2 into Eq. 3.2.5 at steady-state, we find a differential equation describing the evolution for the pump intensity.:

$$\frac{\partial I_p}{\partial z} = -\alpha_{p0} I_p \left(\frac{1 + f_p \dfrac{I_p}{I_{sa}}}{1 + \dfrac{I_p}{I_{sa}}} \right). \tag{3.2.6}$$

Here, α_{p0} is the small-signal differential absorption coefficient at the pump wavelength ($\alpha_{p0} = N_t \sigma_a$). In our experiments, the pump beam has a Gaussian distribution for both cw and pulsed cases. The Gaussian shaped cw pump beam can be expressed in terms of the Gaussian beam parameters as

$$I_p(r,z) = P_p(z)\phi_p(r,z), \tag{3.2.7}$$

where $P_p(z)$ is the pump power at the location z and $\phi_p(r,z)$ is the normalized transverse intensity distribution

$$\phi_p(r,z) = \frac{2}{\pi\omega_p(z)^2} \exp\left(\frac{-2r^2}{\omega_p(z)^2} \right). \tag{3.2.8}$$

In Eq. 3.2.8, $\omega_p(z)$ is the position-dependent spotsize function. If we substitute Eqs. 3.2.7 and 3.2.8 into Eq. 3.2.6 and integrate over the beam cross section, we obtain a differential equation in terms of Gaussian beam parameters which describes the evolution of the pump power inside the saturable absorber:

$$\frac{dP_p}{dz} = -\alpha_{p0} P_p \int_0^{\infty} dr 2\pi r \phi_p \left(\frac{1 + f_p \dfrac{P_p \phi_p}{I_{sa}}}{1 + \dfrac{P_p \phi_p}{I_{sa}}} \right). \tag{3.2.9}$$

In the pulsed case, Eq. 3.2.9 will be written in terms of the integrated pulse energy of the pump beam. The pump photon intensity I_p is related to the integrated pump pulse energy per unit area $\overline{E}_p$ according to

$$\int_{-\infty}^{\tau} dt I_p(t) = \overline{E}_p \,, \tag{3.2.10}$$

where τ is a sufficiently long time at which the pump intensity vanishes and it is assumed to be shorter than the fluorescence lifetime (τ_f) of the upper energy level. Notice that the pump intensity I_p and the electromagnetic energy u_p are related through the equation $I_p = u_p v_g$. If we substitute Eq. 3.2.10 into Eq. 3.2.5 and then integrate with respect to time from $-\infty$ to τ, the following relation is obtained:

$$\frac{\partial \overline{E}_p}{\partial z} = (1 - f_p) h \nu_p \left(N_g(\tau) - N_t \right) - \sigma_{esa} N_t \overline{E}_p \,. \tag{3.2.11}$$

If we assume that $N_g(-\infty)$ is equal to N_t, $N_g(\tau)$ can be expressed in terms of N_t, $\overline{E}_p$ and the absorption saturation energy of the saturable absorber at the pump wavelength ($E_{sa} = h\nu_p / \sigma_a$) as:

$$N_g(\tau) = N_t e^{-\overline{E_p}/E_{sa}} \,. \tag{3.2.12}$$

Similar to the cw case, the integrated pump pulse energy per unit area $\overline{E}_p$ has a Gaussian shape in the following form:

$$\overline{E}_p = E_p(z) \phi_p(r, z) \,. \tag{3.2.13}$$

If we substitute Eq. 3.2.13 into 3.2.11 and integrate over the cross section of the beam then a differential equation describing the pump energy change per unit area in the saturable absorber can be obtained in terms of the total pump energy per pulse E_p:

$$\frac{\partial E_p}{\partial z} = -(1-f_p)h\nu_p \frac{\alpha_{p0}}{\sigma_a}\int_0^\infty dr\, 2\pi r\left(1-\exp\left(-\frac{\sigma_a E_p \phi_p}{h\nu_p}\right)\right) - f_p \alpha_{p0} E_p . \qquad (3.2.14)$$

Equations 3.2.9 and 3.2.14 will be used in the analysis of the experimental saturation data taken with Cr^{2+}:ZnSe samples.

3.3 Passive Q switching

Q switching is one of the techniques that can be used to obtain pulsed laser output. In Q switching of lasers, an optical switch is introduced inside the laser cavity to control the quality factor of the resonator as shown in Figure 3.3. The quality factor determines the lifetime of the laser photons circulating inside the cavity. The higher the quality factor is, the longer the lifetime of the photon packet circulating inside the cavity. When the switch is turned on during the operation of the laser, the quality factor decreases and the threshold increases. Because of that, the laser cannot operate but the gain inside the laser medium builds up. When the switch is turned off, the quality factor of the resonator increases and the gain is depleted via stimulated emission. As a result of this process, a Q-switched pulse is obtained. In our case, a saturable absorber is used as a passive optical switch inside the resonator. Notice that the transmission of the saturable absorber at the laser wavelength depends on the laser photon intensity incident on it. In this section, first the Q-switched pulse formation dynamics will be discussed qualitatively. Then a Q-switched laser model will be presented to drive an expression for the repetition rate of the Q-switched pulse which is a function of the small-signal power gain, fluorescence lifetime, and the small-signal absorption of the saturable absorber. Finally the laser intensity evolution inside the gain medium will be modeled to calculate the small-signal power gain. Note that the model

for the pump photon absorption inside the saturable absorber will be used to describe the absorption of the pump beam inside the gain medium.

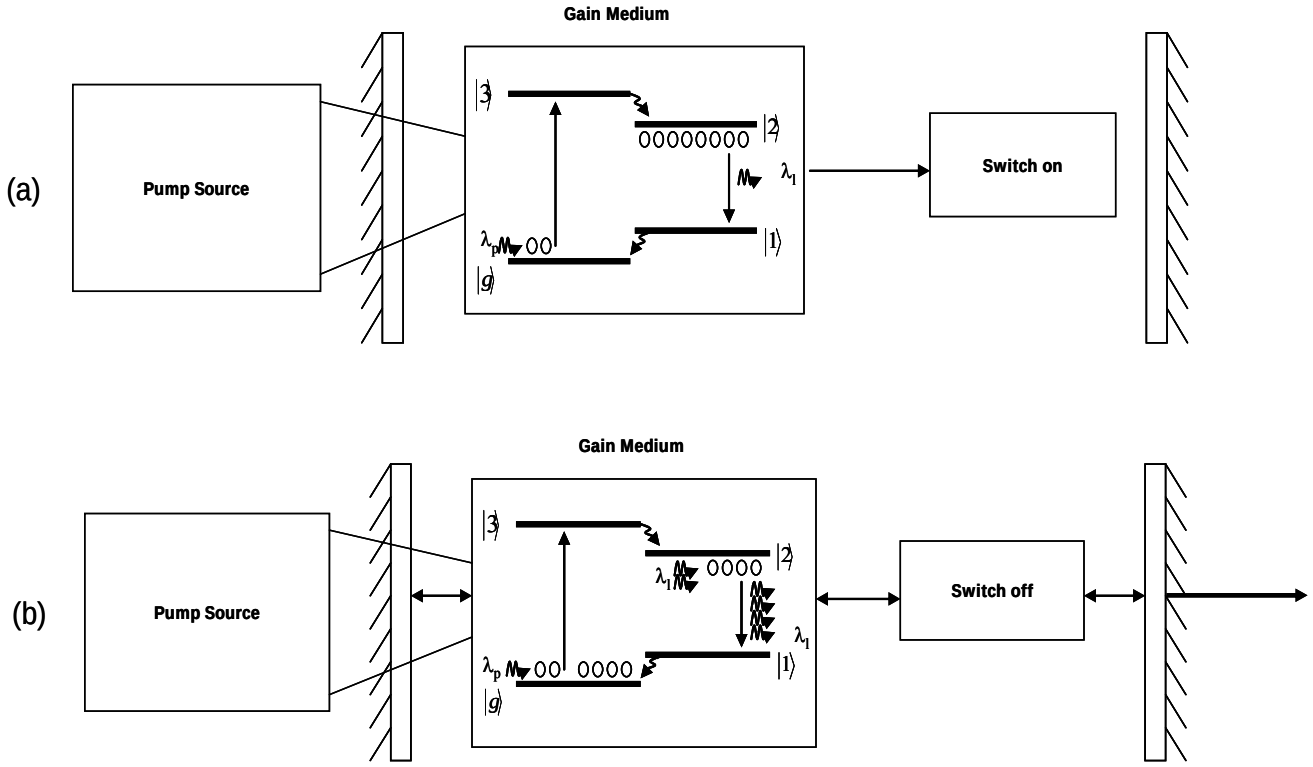

Figure 3.3: A schematic description of Q switching. In (a), when the switch is on, the gain in the gain medium builds up due to the absorption of the pump photons. In (b), when the switch is off, the gain is depleted via stimulated emission.

The pulse forming dynamics will be discussed in four phases as described by Spuhler et al. [33]. In the first phase, the saturable absorber is not bleached yet. The intracavity laser power increases from the noise level until the photon intensity on the saturable absorber is sufficient to saturate the absorber. Note that the saturable absorber is chosen to have less saturation energy than the pulse energy of the laser. In the second phase, the saturable absorber is completely saturated and the intracavity laser intensity grows quickly because

the gain is being depleted by stimulated emission inside the cavity. At the peak of the pulse, the net gain is equal to zero. In the third phase, the net gain becomes negative and the intracavity laser photon intensity decreases. In the fourth phase, the saturable absorber returns to the unsaturated regime before the first phase starts again since the recovery time of the saturable absorber is shorter than the time required for the gain to reach the threshold.

3.3.1 Determination of the Pulse Repetition Frequency

The standard rate equations describing the passively Q-switched lasers can be written as follows:

$$T_R \frac{dP_l(t)}{dt} = \left(g(t) - q(t) - l\right)2P_l(t), \tag{3.3.1.1}$$

$$\frac{dg(t)}{dt} = -\frac{g(t) - g_0}{\tau_l} - \frac{g(t)P_l(t)}{E_L}, \tag{3.3.1.2}$$

$$\frac{dq(t)}{dt} = -\frac{q(t) - q_0}{\tau_f} - \frac{q(t)P_l(t)}{E_A}. \tag{3.3.1.3}$$

Here, P_l is the laser power, g is the single-pass power gain, q is the single-pass saturable loss coefficient, l is the total non-saturable loss coefficient of the cavity, T_R is the cavity round-trip time, τ_l is the fluoresce lifetime of the upper laser level of the gain medium, E_L and E_A are the saturation energies of the gain medium and the saturable absorber, respectively. Eqs. 3.3.1.1, 3.3.1.2 and 3.3.1.3 are valid for the case where g, q and l are small. During the pulse formation, the relaxation time of the saturable absorber and the pumping of the gain medium can be neglected. Then Eqs. 3.3.1.2 and 3.3.1.3 are simplified to:

$$\frac{dg(t)}{dt} = -\frac{g(t)P_l(t)}{E_L}, \tag{3.3.1.4}$$

$$\frac{dq(t)}{dt} = -\frac{q(t)P_l(t)}{E_A}. \tag{3.3.1.5}$$

The ratio of Eqs. 3.3.1.4 to 3.3.1.5 gives a relation between g and q in terms of the initial conditions of g (g_i) and q (q_0)

$$q = q_0\left(g/g_i\right)^{E_L/E_A}. \tag{3.3.1.6}$$

Similarly, if we divide Eq. 3.3.1.1 by Eq. 3.3.1.4 and use Eq. 3.3.1.6, we can express P_l as a function of the gain during the Q-switch cycle:

$$P_l(g) = -\frac{2E_L}{T_R}(g - g_i) + \frac{2lE_L}{T_R}\ln\left(\frac{g}{g_i}\right) + \frac{2E_A q_0}{T_R}\left[\left(\frac{g}{g_i}\right)^{E_L/E_A} - 1\right]. \tag{3.3.1.7}$$

Before and after the Q-switched pulse, the laser power inside the cavity is approximately zero. According to this assumption, Eq. 3.3.1.7 gives an expression as a function of the initial and the final gain (g_f):

$$P_l(g_f) = 0 = g_i - g_f + l\ln\left(\frac{g_f}{g_i}\right) + \frac{E_A q_0}{E_L}\left[\left(\frac{g_f}{g_i}\right)^{E_L/E_A} - 1\right]. \tag{3.3.1.8}$$

Notice that the saturation energy of the gain medium is greater than the saturation energy of the saturable absorber. Because of that, we can neglect the last term in Eq. 3.3.1.8 and arrive at an approximate expression for the gain reduction ($\Delta g = g_i - g_f$):

$$\Delta g \approx -l\ln\left(\frac{l + q_0 - \Delta g}{l + q_0}\right). \tag{3.3.1.9}$$

Spuhler et al. [33] obtained the numerical solution of Eq. 3.3.1.9 for Δg as a function of l for several values of q_0. In our case, l (0.02) is very small comparison to q_0 (0.2). The numerical solution indicates that when $l/q_0 << 1$, Δg is approximately equal to q_0.

In order to obtain an expression for the repetition frequency (f_{rep}) of the Q-switched pulse, we can divide the average output power (P_{av}) by the output pulse energy (E_p). The average output energy can be expressed in terms of the pump power (P_p), the threshold pump power ($\left(P_p\right)_{th}$) and the slope efficiency of the laser (η_s) as:

$$P_{av} = \eta_s \left(P_p - \left(P_p\right)_{th}\right). \tag{3.3.1.10}$$

P_p is proportional to the small-signal gain coefficient (g_0) according to

$$P_p = \frac{h\nu_p}{\sigma_e \tau_f \eta_p} g_0 . \tag{3.3.1.11}$$

Here, $h\nu_p$ is the pump photon energy, σ_e is the emission cross section of the gain medium, and η_p is the pumping efficiency. At threshold, the small-signal gain is equal to the total loss of the cavity ($g_0 = l + q_0$). The output pulse energy can be obtained from the stored energy (E_{st}) in the laser cavity. E_{st} is proportional to the laser photon energy ($h\nu_l$), ion density in the second energy level of the gain medium (N_2) and the pumped volume (AL_g):

$$E_{st} = h\nu_l N_2 A L_g . \tag{3.3.1.12}$$

For a standing-wave cavity, the single-pass power gain can be expressed as:

$$g = \sigma_e N_2 L_g . \tag{3.3.1.13}$$

Here, σ_e is the emission cross section of the gain medium. If we substitute Eq. 3.3.1.13 into Eq. 3.3.1.12, we obtain

$$E_{st} = \frac{h\nu_l A}{\sigma_e} g \,. \tag{3.3.1.14}$$

The released energy is equal to the difference between the initial and the final stored energy. The output pulse energy is obtained by multiplying released energy with output coupling efficiency. If a Q-switched pulse reduces the net gain by Δg, the pulse energy is expressed as

$$E_p = \frac{h\nu_l A}{\sigma_e} \Delta g \frac{l_{out}}{l}, \tag{3.3.1.15}$$

where l_{out} is the output coupling coefficient. Notice that the repetition rate of the Q-switched pulse can be found by the relation

$$f_{rep} = \frac{P_{av}}{E_p} = \frac{\eta_s \left(P_p - \left(P_p\right)_{th}\right)}{E_p}. \tag{3.3.1.16}$$

If we assume that decay rate due to spontaneous emission ($AL_g N_2 / \tau_f$) is compensated by the pump rate ($\eta_p P_p / h\nu_p$), we can obtain the following expression for f_{rep} by using Eqs. 3.3.1.11, 3.3.1.15, and 3.3.1.16:

$$f_{rep} = \frac{g_0 - \left(l + q_0\right)}{\Delta g \tau_f}. \tag{3.3.1.17}$$

In our case, we assumed that the final depleted gain is negligible and the single pass non-saturable cavity loss is very small in comparison with the single-pass small-signal loss of the saturable absorber. Notice that the numerical solution of Eq. 3.3.1.9 indicates that Δg is approximately equal to q_0 for small l values [33]. Therefore, we can use an approximate expression to model the repetition rate as:

$$f_{rep} \approx \frac{g_0 - q_0}{q_0 \tau_f}. \tag{3.3.1.18}$$

τ_f and q_0 can be experimentally measured parameters. In Eq. 3.3.1.18, g_0 is the only unknown parameter.

3.3.2 Determination of g_0

In order to determine g_0, the laser power evolution inside the gain medium will be modeled for the cw case. In the model, a 4-level energy system of the gain medium is assumed. The energy levels in the gain medium are similar to those of the saturable absorber but now we are interested in not only absorption of the pump power but also the interaction of the laser photons with the gain medium. Because of that, we will use Eq. 3.1.1 without neglecting stimulated emission term. For steady-state case, Eq. 3.1.1 gives the relation between N_2 and N_1

$$N_2 = N_t \frac{\frac{I_p}{I_{sa}}}{1+\frac{I_p}{I_{sa}}+\frac{I_l}{I_{se}}}, \qquad (3.3.2.1)$$

where I_{se} is the saturation intensity of emission ($I_{se} = h\nu_l / \sigma_e \tau_f$). I_l is the sum of two photon intensities propagating in the directions $+z$ and $-z$ namely I_l^+ and I_l^-, respectively. Consider a gain medium with a cross sectional area A and an infinitesimal length, dz, as shown in Figure 3.4:

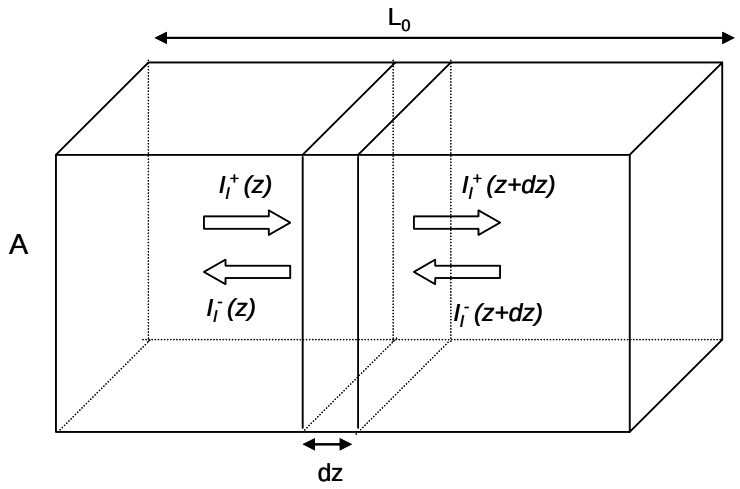

Figure 3.4: Laser beam evolution inside the laser gain medium.

The conservation of energy gives the following relation for the laser photon intensity propagating in $+z$ direction (I_l^+):

$$Adz\frac{\partial u_l}{\partial t} = \left(I_l^+(z) - I_l^+(z+dz)\right)A - \left(-N_2\sigma_e I_l^+ + N_2(\sigma_{esa})_l I_l^+\right)Adz\,. \qquad (3.3.2.2)$$

Here, u_l is the electromagnetic energy density and $(\sigma_{esa})_l$ is the excited-state absorption cross section at the laser wavelength. In Eq. 3.3.2.2, the spontaneous emission is neglected and the loss inside the medium is assumed to be due to the excited-state absorption at the laser wavelength inside the gain medium. Note that the electromagnetic energy density is related to the laser photon intensity by $u_l = v_g I_l$. Eqs. 3.3.2.1 and 3.3.2.2 give a relation for the laser photon intensity propagating in the $+z$ direction for the steady-state case:

$$\frac{\partial I_l^+}{\partial z} = (1-f_l)\sigma_e I_l^+ N_t \frac{\dfrac{I_p}{I_{sa}}}{1+\dfrac{I_p}{I_{sa}}+\dfrac{I_l}{I_{se}}}\,. \qquad (3.3.2.3)$$

In Eq. 3.3.2.3, f_l is the normalized excited-state absorption coefficient at the laser wavelength $f_l = (\sigma_{esa})_l / \sigma_e$. In our case, we will assume a Gaussian beam distribution for the pump and the laser beams inside the gain medium similar to the analysis of saturable absorbers. Eq. 3.3.2.3 can be used to obtain the evolution equation for the laser beam power in terms of the Gaussian beam parameters as

$$\frac{dP_l^+}{dz} = \sigma_e N_t (1 - f_l) \int_0^\infty dr 2\pi r \left(\frac{\frac{P_l^+ P_p \phi_l \phi_p}{I_{sa}}}{1 + \frac{P_p \phi_p}{I_{sa}} + \frac{P_l \phi_l}{I_{se}}} \right), \tag{3.3.2.4}$$

where ϕ_l is the normalized transverse intensity distribution of the laser beam. When we ignore the pump saturation and the excited-state absorption at the pump wavelength, Eq. 3.2.9 can be expressed in terms of the incident pump power P_{pi} ($P_{pi} = P_p(z=0)$)

$$P_p(z) = P_{pi} \exp(-\alpha_{p0} z). \tag{3.3.2.5}$$

The evolution of the laser power propagating to $+z$ direction inside the gain medium can be described by the following differential equation when I_{se} is neglected:

$$\frac{dP_l^+}{dz} = \sigma_e N_t (1 - f_l) \int_0^\infty dr 2\pi r \left(\frac{\frac{P_l^+ P_{pi} \phi_l \phi_p \exp(-\alpha_{p0} z)}{I_{sa}}}{1 + \frac{P_{pi} \phi_p \exp(-\alpha_{p0} z)}{I_{sa}}} \right). \tag{3.3.2.6}$$

By solving Eq. 3.3.2.6, we can determine the intracavity laser power at any point inside the gain medium. The single-pass gain (g_0) can be calculated by using the laser power values at the edges of the gain medium with length L_0:

$$g_0 = \frac{P_l^+(L_0) - P_l^+(0)}{P_l^+(0)}. \tag{3.3.2.7}$$

Therefore, we can theoretically calculate the repetition rate of a passively Q-switched laser by using Eqs. 3.3.1.18, 3.3.2.6 and 3.3.2.7.

Chapter 4

EXPERIMENTAL DETERMINATION OF THE SATURATION PARAMETERS FOR Cr^{2+}:ZnSe

4.1 Introduction:

The saturation parameters of five Cr^{2+}:ZnSe samples were determined at the wavelengths of 1570 and 1800 nm experimentally. In the analysis of the experimental data, we used the models discussed in the previous chapter. A best-fit algorithm was employed to determine the ground-state and excited-state absorption cross sections. In this section, the procedure for the determination of the saturation parameters of Cr^{2+}:ZnSe will be explained and the obtained results will be compared with the previously reported values in the literature. The organization of this chapter is as follows: First, the experimental setup of the two pumping configurations will be explained. Then, the best-fit algorithm used in the analysis of the experimental data will be discussed. Then, a similar analysis will be carried out for the pulsed case and the average σ_a values at 1800 nm and 1570 nm will be compared with the average of the previously reported values. Finally, the consistency of σ_a values at 1800 nm and 1570 nm will be evaluated by using the absorption spectrum of Cr^{2+}:ZnSe.

4.2 Experimental Setups

The schematic of the experimental setup for the continuous-wave (cw) bleaching of Cr^{2+}:ZnSe is shown in Figure 4.1.

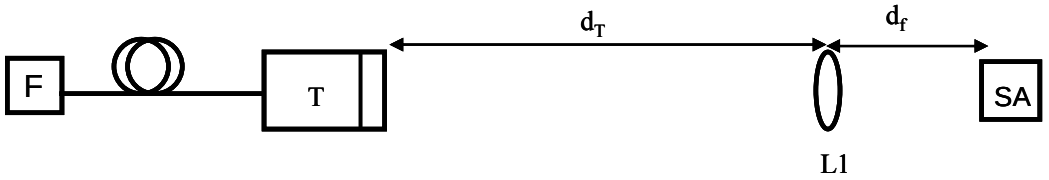

Figure 4.1: Experimental setup of cw bleaching experiment.

In the cw bleaching experiments, a commercial Thulium doped fiber laser (F) operating at 1800 nm (IPG Laser thulium fiber laser) was used as the pump source. The laser light was focused on the saturable absorber by using an anti-reflection (AR) coated lens at 1800 nm (L1). The focal length of the lens was 10 cm. The lens was positioned 168 cm away from the output of the fiber laser. The spotsize of the focused light was measured by using the knife-edge method. In particular, the beam cross section was scanned by a vertically positioned sharp blade to determine the positions giving %84 and % 16 power transmissions at different positions. The distance between these positions gives the spotsize at that particular position on the optical axis. The following functional form was assumed for the beam spotsize in order to determine the beam waist:

$$\omega(z) = \omega_0 \sqrt{1 + \left(\frac{z - z_f}{z_R} \right)^2} \quad . \tag{4.2.1}$$

Here, ω_0 is the beam waist, z_R is the Rayleigh range and z_f is the beam waist location. The beam waist was determined to be 28.6 μm by using a best-fit algorithm. The Cr^{2+}:ZnSe samples were held inside an aluminum holder which was maintained at a temperature of 20˚C. The sample was put to the focal point of the lens at Brewster angle to minimize the reflection losses from the surfaces. The cylindrical polycrystalline ZnSe substrates were supplied by Crystran Ltd. and chromium was added by the diffusion doping technique (See Ref [2]). Table 4.1 summarizes some of the optical and physical properties of the Cr^{2+}:ZnSe samples. In the experiments, the incident and transmitted laser power levels were measured with a power meter (Coherent, Model PowerMax 5200).

Cr^{2+}:ZnSe Sample No	Diameter (mm)	Crystal Length (mm)	Lifetime (μs)	α_{p0} at 1800 nm (m^{-1}) (Spectrometer value)	α_{p0} at 1570 nm (m^{-1}) (Spectrometer value)
1	10	1.92	5.1	307.6	120.8
2	10	2.00	5.1	448.1	176.0
3	10	1.94	5	638.7	250.9
4	10	1.85	4.3	1198.8	470.9
5	10	1.77	4.3	956.1	375.6

Table 4.1: Optical and physical properties of cylindrical polycrystalline Cr^{2+}:ZnSe samples.

In the pulsed bleaching experiments at 1570 nm, an extra cavity optical parametric oscillator (OPO) was used as the pump source. The OPO was operated at the repetition rate of 1 kHz. The OPO setup consisted of an optical cavity and a KTP crystal. The sketch of the experimental setup and the photograph of the OPO cavity are shown in Figures 4.2 (a) and (b), respectively.

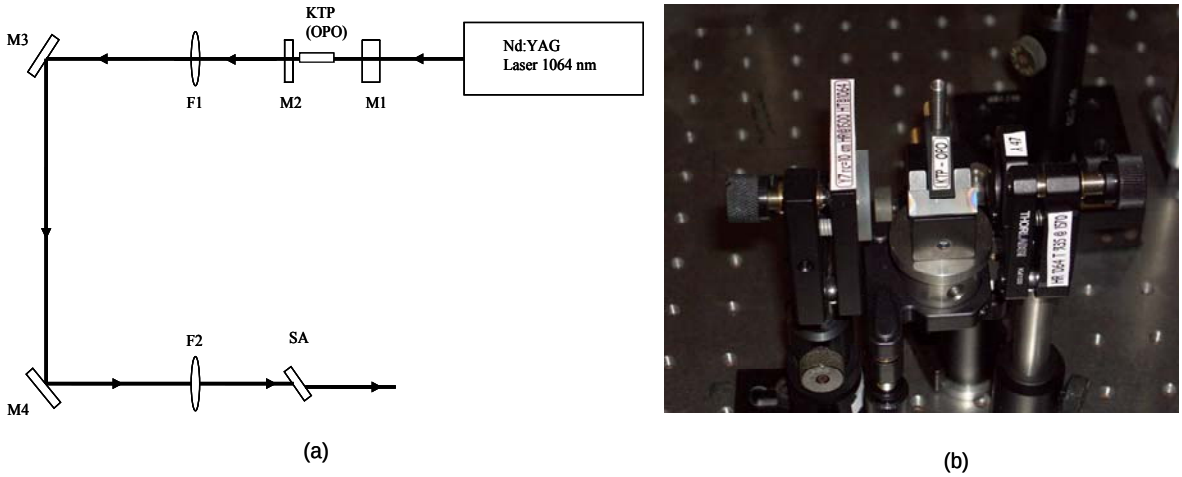

Figure 4.2: (a) Sketch of the experimental setup of the pulsed bleaching experiment. (b) Photograph of the KTP OPO operating at 1570 nm.

The KTP OPO crystal was pumped by a commercial Nd:YAG laser (Quantronix 116) producing Q-switched pulses at 1064 nm. The output pulsewidth of the OPO was 65 ns. The OPO output was collimated by a converging lens with 20 cm focal length (F1). Two dichronic mirrors highly reflective at 1570nm and highly transitive at 1064 nm (M3 and

M4) were used to filter out the laser light at 1570 nm. The collimated output of the OPO was focused into the Cr^{2+}:ZnSe sample by an anti-reflection coated lens with a focal length of 10 cm (F2). The sample was positioned at Brewster angle to minimize surface reflections. The beam waist of the focused light was determined to be 69.5 μm by using the knife-edge method discussed above for the cw case.

The lifetime measurements of the Cr^{2+}:ZnSe samples were carried out by using the KTP OPO system employed in the pulsed bleaching experiments. The output of the OPO was focused into the samples by a converging lens with 5-cm focal length. The signal was collected with a MgF_2 lens (f=8 cm) and the fluorescence decay signal was filtered out from the pump laser by using several high-pass filters. The signal was measured with a fast InGaAs detector which was sensitive to radiation between 1.2 and 2.6 μm (response time = 3 ns) and recorded with a digital sampling oscilloscope. The absorption spectrum measurements were performed by a commercial spectrometer (Shimadzu UV-VIS-NIR 3101 PC).

4.3 Results and Discussion

The saturation parameters (σ_a and f_p) of Cr^{2+}:ZnSe were determined by using two different methods for the cw case at 1800 nm and the pulsed case at 1570 nm. In both methods, the transmission of the pump laser light through the saturable absorber samples was measured with respect to the pump photon intensity incident on the samples. In the first method, the pump photon intensity was controlled by varying the incident pump power on the sample. In the second method (z-scan method), the intensity was controlled by changing the spotsize of the laser beam on the samples for a constant incident pump power. The spotsize was varied by translating the samples along the optical axis. The obtained experimental data were analyzed by using a best-fit algorithm for both methods.

4.3.1 Continuous-Wave Case

In the best-fit analysis of the cw case, Eq. 3.2.9 was used to model the saturation of Cr^{2+}:ZnSe. In the first step of the best-fit algorithm, Eq. 3.2.9 is solved for an initial σ_a, α_0 and f_p values and the standard deviation between the experimental and the theoretical transmission is calculated. Then, the procedure is iterated by changing σ_a, α_0 and f_p until the standard deviation is minimized. By this way, the best-fit values of σ_a, α_0, f_p are determined. Note that the Cr^{2+} concentration in the Cr^{2+}:ZnSe samples is not homogeneous close to the edge of the unpolished surfaces due to the nature of diffusion doping. The absorption spectrum measurement determines the average α_0 over the sample surface. In the analysis of both experimental methods, α_0 was employed as a fitting parameter to be more accurate in the determination of the saturation parameters.

The best-fit algorithm was applied for an array of the incident pump power values for the first experimental method. On the other hand, in the analysis of the z-scan method, the best-fit algorithm was employed for a constant pump power with different spotsize values. Figure 4.3 shows the measured and calculated transmission results of sample 1 for both methods.

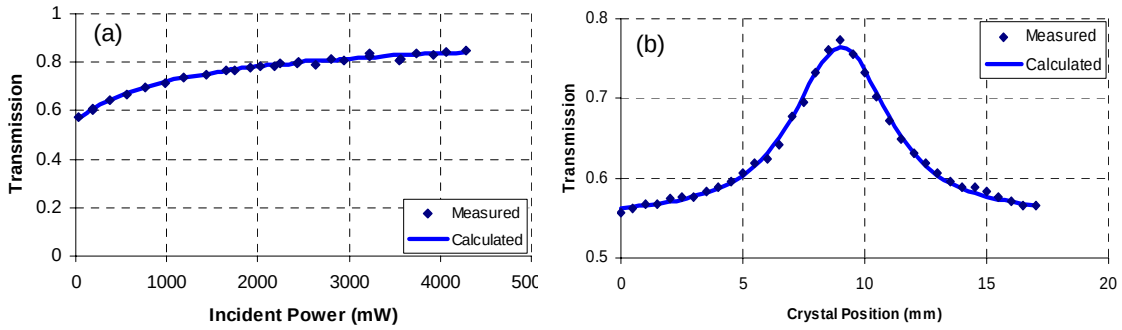

Figure 4.3: Measured and calculated transmission as a function of the (a) incident power and (b) crystal position (incident pump power=1700 mW) at 1800 nm. Cr^{2+}:ZnSe sample 1 (see Table 4.1) was used.

Here, the Cr^{2+}:ZnSe sample used had the following properties: length=1.92 mm, τ_f = 5.1 μm, α_{p0} at 1570 nm=120.8 m^{-1}.Tables 4.2 and 4.3 summarize the best-fit saturation parameters of the five Cr^{2+}:ZnSe samples for the first and second methods, respectively. The average best-fit σ_a value of the Cr^{2+}:ZnSe samples for the first method ($6.28x10^{-19}$ cm^2) is very close the average value for the second method ($6.05x10^{-19}$ cm^2). The average percentage deviation of the best-fit α_0 value from the absorption measurements is about 5 % for two methods. The obtained f_p values in both methods indicate that the excited-state absorption is negligible as found in the other references [26, 28, 29, 34]

Cr^{2+}:ZnSe Sample No	**α_{p0} at 1800 nm (m^{-1}) (Spectrometer value)**	**α_{p0} at 1800 nm (m^{-1}) (Best-fit value)**	f_p	**σ_a at 1800nm (x 10^{-23} m^2)**
1	307.6	279.0	0.07	7.09
2	448.1	454.0	0.04	5.04
3	638.7	665.0	0.03	4.58
4	1198.8	1102.0	0.14	8.66
5	956.1	996.0	0.04	6.05
	Mean		0.06	6.28

Table 4.2: The best-fit saturation parameters of the Cr^{2+}:ZnSe samples at 1800 nm for the first method.

Cr^{2+}:ZnSe Sample No	**α_{p0} at 1800 nm (m^{-1}) (Spectrometer value)**	**α_{p0} at 1800 nm (m^{-1}) (Best-fit value)**	f_p	**σ_a at 1800nm (x 10^{-23} m^2)**
1	307.6	288.0	0.00	6.90
2	448.1	455.0	0.00	5.95
3	638.7	656.0	0.00	5.85
4	1198.8	1067.0	0.00	6.05
5	956.1	977.0	0.00	5.50
	Mean		0.00	6.05

Table 4.3: The best-fit saturation parameters of the Cr^{2+}:ZnSe samples at 1800 nm for the second method (z-scan method) are summarized.

4.3.2 Pulsed Case

Similar to the cw case, a best-fit algorithm was employed in the analysis of the experimental results but in this case, the algorithm numerically solved Eq. 3.2.14 to obtain the saturation parameters. In addition, in the analysis of the z-scan measurements, α_{p0} value was kept fixed at the value obtained from the absorption spectrum measurements because the small-signal transmission data were not sufficient to estimate α_{p0} by fitting the theoretical transmission to the experimental data. In the analysis of the first method, α_{p0} was taken as the best-fit parameter similar to the cw case and the average percentage deviation of the spectrometer α_{p0} value from the best-fit result was determined to be 5.02 %. Figures 4.4 (a) and (b) show the experimental and the best-fit transmission results for the both methods and the best-fit saturation parameters at 1570 nm are summarized in Tables 4.4 and 4.5 The average best-fit σ_a values for the first and second methods (2.24×10^{-23} and 2.23×10^{-23} m^2, respectively) are in very good agreement and the average f_p values for both methods (0.08 for the first method, 0 for the second method) indicate that the excited-state absorption is negligible similar to the cw case.

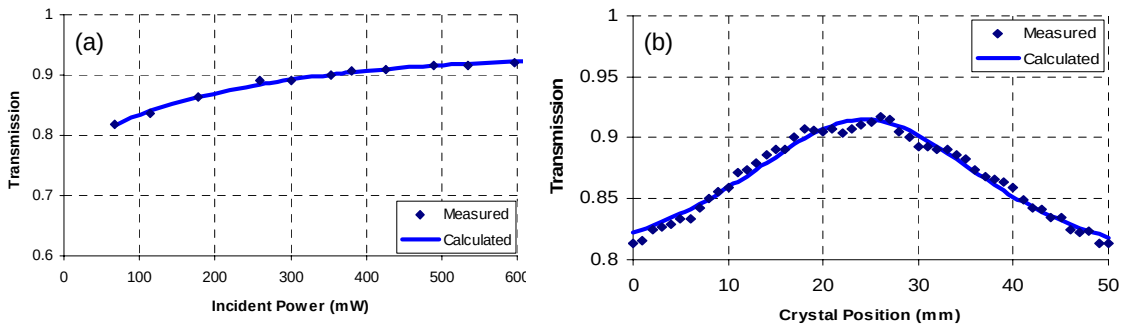

Figure 4.4: Measured and calculated transmission as a function of the (a) incident power and (b) crystal position (incident pump power=490 mW) at 1570 nm. Cr^{2+}:ZnSe sample 1 (see Table 4.1) was used.

Cr^{2+}:ZnSe Sample No	**α_{p0} at 1570 nm (m^{-1}) (Spectrometer value)**	**α_{p0} at 1570 nm (m^{-1}) (Best-fit value)**	f_p	**σ_a at 1570nm (x 10^{-23} m^2)**
1	120.8	128.4	0.08	2.20
2	176.0	176.4	0.19	3.02
3	250.9	232.7	0.00	1.38
4	470.9	473.7	0.06	2.15
5	375.6	415.6	0.08	2.46
		Mean	0.08	2.24

Table 4.4: The best-fit saturation parameters of the Cr^{2+}:ZnSe samples at 1570 nm for the first method.

Cr^{2+}:ZnSe Sample No	**α_{p0} at 1570 nm (m^{-1}) (Spectrometer value)**	f_p	**σ_a at 1570nm (x 10^{-23} m^2)**
1	120.8	0.0	1.90
2	176.0	0.0	2.70
3	250.9	0.0	2.00
4	470.9	0.0	2.00
5	375.6	0.0	2.55
	Mean	0.00	2.23

Table 4.5: The best-fit saturation parameters of the Cr^{2+}:ZnSe samples at 1570 nm for the second method (z-scan method).

Table 2.2 shows the σ_a values in the literature at different wavelengths and the estimated σ_a at 1800 nm and 1570 nm according to the spectral absorption measurement of Cr^{2+}:ZnSe sample 5 (see Table 4.1)shown in Figure 4.5.

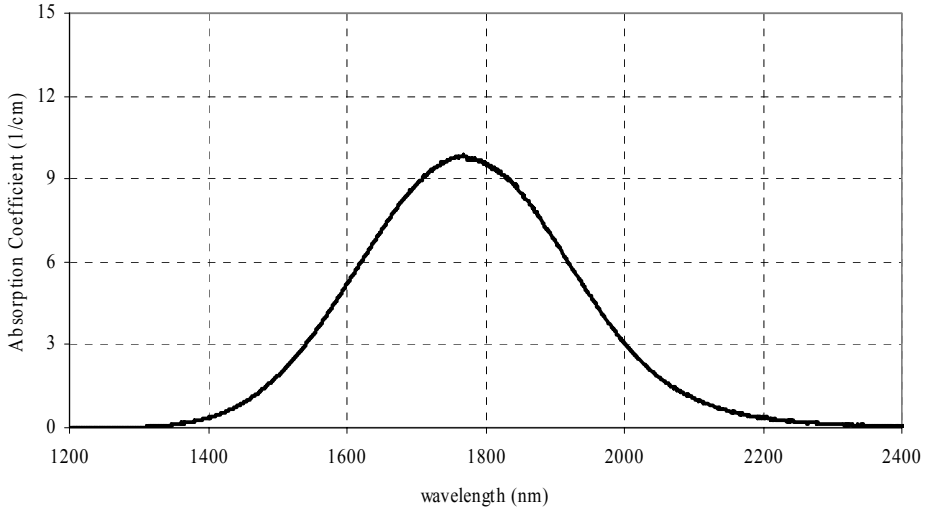

Figure 4.5: Absorption spectrum of Cr^{+2}:ZnSe sample 5.

The average best-fit σ_a values at the wavelengths 1800 nm and 1570 nm (6.17×10^{-19} cm^2 and 2.24×10^{-19} cm^2, respectively) are below the average of the previously reported values ($12..1 \times 10^{-19}$ cm^2 and 4.7×10^{-19} cm^2, respectively). The difference between the obtained value and the values in the references [1, 23, 25-30] might be due to the polycrystalline structure of our samples. However the average best-fit σ_a results of two methods at two wavelengths are consistent with each other according to the spectrometer measurement of the absorption coefficient shown in Figure 4.5. In order to check the consistency, the ratio of the average best-fit σ_a values at two wavelengths ($(\sigma_a)_{1800}/(\sigma_a)_{1570} = 2.75$) were compared with the ratio of the absorption coefficients ($(\alpha_{p0})_{1800}/(\alpha_{p0})_{1570} = 2.55$) at the particular wavelengths. The percentage deviation of the best-fit ratio from the spectral absorption measurement was 8 %.

Chapter 5

APPLICATION OF Cr^{4+}:YAG SATURABLE ABSORBERS IN PASSIVE Q SWITCHING

5.1 Introduction

Up to now, we discussed the model for a four-level saturable absorber, the mechanism of passive Q switching of a laser and we described the experimental determination of the ground-state and excited-state absorption cross sections of Cr^{2+}:ZnSe saturable absorbers. In this section, we will focus on two applications of Cr^{4+}:YAG saturable absorbers in passive Q switching of solid-state lasers. In the first application, a cw-pumped passively Q-switched Nd^{3+}:YVO_4 laser will be demonstrated. Then, the repetition rate of the pulses will be analyzed by using the previously derived model. In the second application, a flashlamp-pumped passively Q-switched Nd:YAG will be described.

5.2 Passive Q Switching of cw-pumped Nd^{3+}:YVO_4 Laser:

In this part of the thesis, the application of the Cr^{4+}:YAG saturable absorber in passive Q switching of a cw-pumped Nd^{3+}:YVO_4 laser will be shown and then a control method of the pulse repetition rate will be discussed. The control of the repetition rate can be achieved by using a lens inside the resonator. When we translate the lens along the optical axis, the mode matching of the pump and the laser beams inside the gain medium can be changed and the single-pass power gain can be varied. As a result of this, the repetition rate of the Q-switched pulses can be changed. The organization of this section is as follows. First, the

experimental setup will be described and the results will be presented. In particular, the variation of the average output power, the repetition rate and the pulse width of the Q-switched pulses will be shown as a function of the incident pump power. Then, the effect of the intracavity lens position on the repetition rate will be discussed. Second, the rate equation analysis will be employed in the analysis of the repetition rate control data and the emission cross section of the gain medium will be determined by a best-fit algorithm.

5.2.1 Experimental Setup and Results

Figure 5.1 shows the experimental setup. The laser cavity consisted of a 10 mm-long a-cut Nd^{3+}-doped YVO_4 crystal as the gain medium, a flat 2.2 % transmitting output coupler (OC), an antireflection coated intracavity lens with the focal length of 10 cm (L1), and a Cr^{4+}:YAG saturable absorber (SA). The Nd^{3+} concentration in the YVO_4 crystal was 0.5 at. %. The Nd^{3+}:YVO_4 crystal was held inside a copper block and the temperature of the block was maintained at 18 ˚C. In order to increase the heat conduction between the Nd^{3+}:YVO_4 crystal and the copper block, the crystal was wrapped in tin foil.

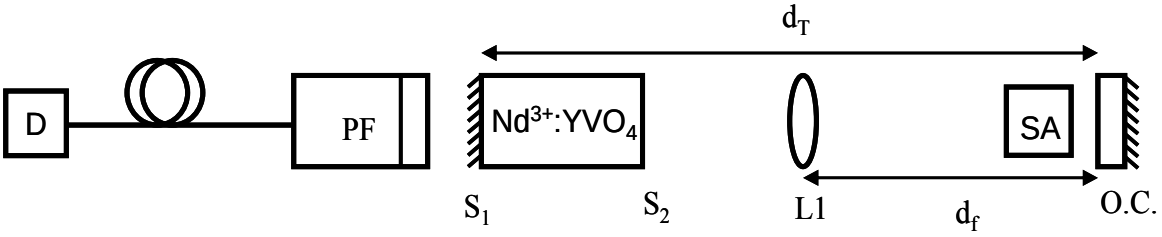

Figure 5.1: Schematic of the diode-pumped passively q-switched Nd^{3+}:YVO_4 laser.

One surface of the crystal was highly reflective at 1064 nm and highly transitive at 809 nm. The other surface was antireflection coated at 1064 nm. The length of the optical resonator (d_T) was 15.2 cm. The intracavity lens was positioned around the center of the resonator. During the experiments, the lens was translated along the optical axis to control the repetition rate of the Q-switched pulses. 1.56-mm-long normal-cut Cr^{4+}:YAG saturable

absorber was positioned near the output coupler. The surfaces of the Cr^{4+}:YAG crystal were antireflection coated at 1064 nm and the small-signal transmission of the crystal was 80 % at 1064 nm. The laser crystal was pumped by a diode-array (D) operating at 806 nm. The output of the diode was coupled by using a 1550-μm-diameter fiber bundle and the output was focused inside the gain medium by using a telescope (PF). The beam waist of the focused light was determined to be 287 μm by the knife-edge technique described in the previous chapter.

The laser experiments were performed in two steps. In the first step, the output power, the repetition rate and the pulse width of the Q-switched pulses were measured as a function of the incident pump power for a fixed intracavity lens position (d_f=9.5 cm). In the second step, the repetition rate was varied by translating the lens along the optical axis inside the cavity for a fixed pump power (P_p =5.4 W). Figures 5.2 (a), (b), and (c) show the variation of the average output power, the repetition rate, and the pulsewidth as a function of the incident pump power, respectively, for the case where the lens was kept fixed at 9.5 cm away from the output coupler.

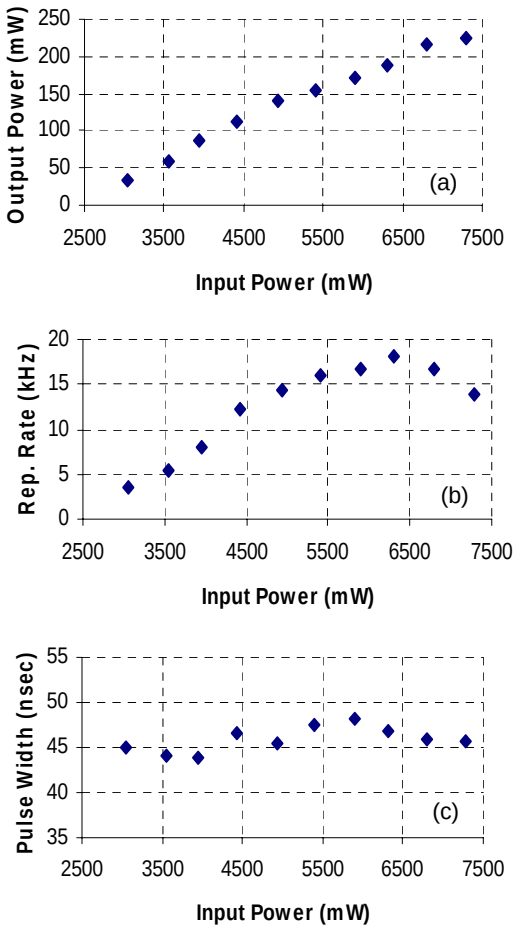

Figures 5.2 (a), (b), and (c) show the variation of the average output power, the repetition rate, and the pulsewidth as a function of the incident pump power at the fixed lens position (d_f=9.5 cm), respectively.

In these measurements, as the pump power was increased from 3.05 to 7.29 W, the repetition rate first increased from 3.5 to 18.2 kHz and then decreased to 13.8 kHz. The pulsewidth remained near 45 ns in this pump power range. As high as 225 mW of average output power was obtained which corresponds to a peak power of 360 W and a pulse energy of 16.3 μJ. In the second step of the measurements, the intracavity lens was

translated from d_f=8.5 cm to d_f= 9.5 cm at a constant pump power of 5.4 W. As shown in Figure 5.3 (a), the repetition rate could be varied in the range between 25 and 18 kHz. By this way, the gain per pulse was changed and as a result of this, the average output power and the pulse width were also affected. (See Figures 5.3 (b) and (c)) The pulse width remained below 100 ns in this range of d_f values.

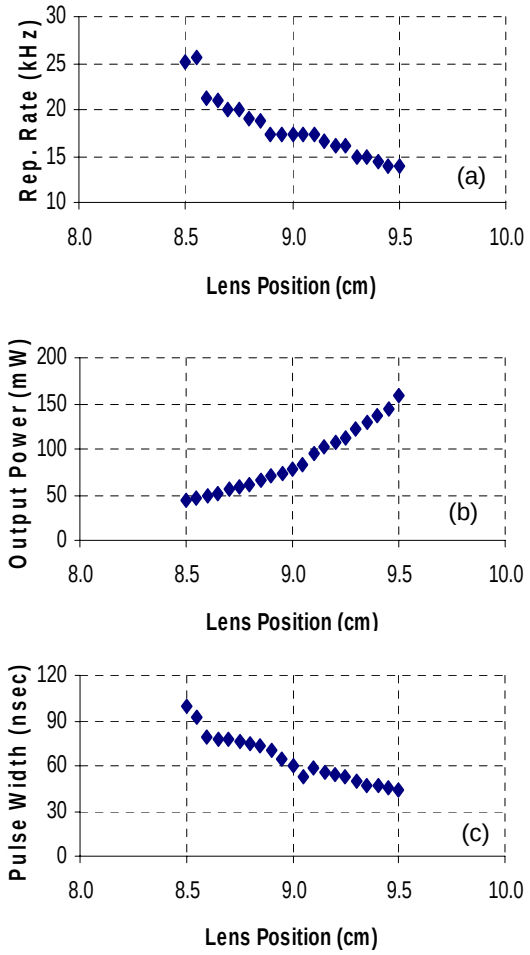

Figures 5.3 (a), (b), and (c) show the variation of the average output power, repetition rate, and the pulsewidth as a function of the intracavity lens position at fixed incident pump power of 5.4 W, respectively.

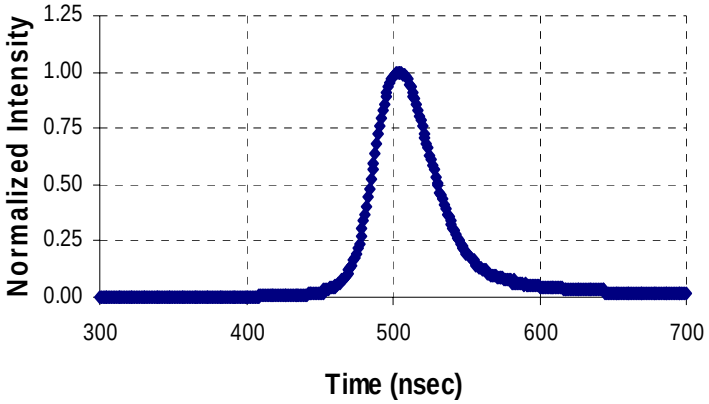

Figure 5.4: Temporal trace of the Q-switched pulse when the intracavity lens was 9.5 cm way from the output coupler. The pulsewidth (FWHM) was 46 ns.

5.2.2 Analysis of the Experimental Results

In the analysis of the cw pumped passively Q-switched Nd^{3+}:YVO_4, the rate equation approach will be employed. Previously, the rate equation formalism was described and a relation for the repetition rate of Q-switched pulses and the steady-state single-pass power gain (g_0) was derived. In this section, these results will be used in the analysis of the repetition rate of the Q-switched pulses. As can be seen from Eq. 3.3.1.18, the repetition rate (f_{rep}) depends on g_0 which is affected by many parameters such as the stimulated emission cross section of the gain medium (σ_e), the fluorescence lifetime (τ_f), the pump power (P_p), and the mode matching of the pump and the laser beams (see Eqs. 3.3.2.6 and 3.3.2.7). In our case, as the intracavity lens was translated, the degree of the overlap between the pump and the laser modes was changed. As a result of that, g_0 was varied with respect to the lens position, hence affecting the repetition rate. In the analysis, the laser spotsize distribution in the gain medium was determined for each intracavity lens

position by using a standard ABCD cavity analysis. Then, for the particular pump and laser spotsize distribution, g_0 was calculated by numerically solving Eq. 3.3.2.6 and the corresponding repetition rate was calculated. A best-fit algorithm was employed to fit the theoretical model to the experimental results. In the algorithm, σ_e and the beam waist location of the pump (z_{fp}) are used as the fitting parameters. Figure 5.5 shows the experimental and calculated repetition rates as a function of the lens position.

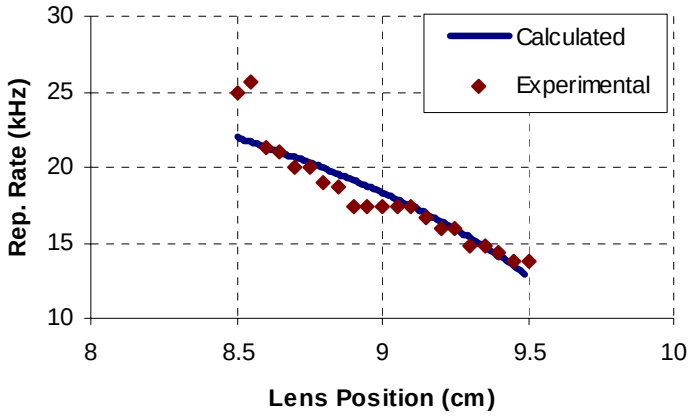

Figure 5.5: Variation of the calculated and measured repetition rate as a function of lens position at the input pump power of 5.4 W.

As a result of the best-fit analysis, z_{fp} and σ_e were determined to be 0.0016 m and 7.7×10^{-19} cm^2, respectively. The obtained best-fit value of σ_e is also consistent with the previously reported value determined by using the cw efficiency data [35].

5.3 Passive Q Switching of Flashlamp-pumped Nd:YAG Laser:

In this section, we will discuss the operation of a passively Q-switched flashlamp-pumped Nd:YAG laser. This laser system is different from the previously discussed laser system in

terms of the pumping mechanism, the gain medium and the output pulse energy scale. Figure 5.6 shows the schematic of the passively flashlamp-pumped Nd:YAG laser.

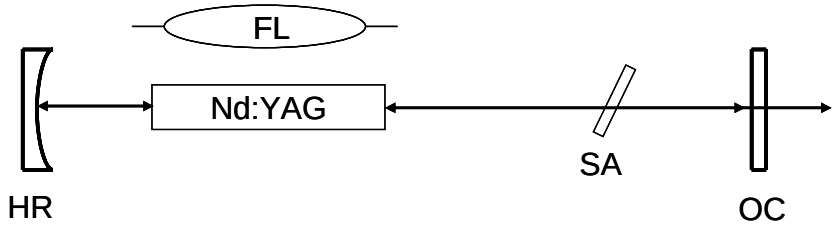

Figure 5.6: Schematic of the flashlamp-pumped passively Q-switched Nd:YAG laser.Q-switched

The laser cavity consisted of a Nd^{3+}-doped YAG crystal as the gain medium, a flat 12 % transmitting output coupler (OC), a curved high reflector at 1064 nm with 100 cm of radius of curvature (HR), and a Cr^{4+}:YAG saturable absorber (SA). The length of the laser cavity was about 32.1 cm. The Nd^{3+} concentration in the YAG crystal was 0.9 at. %. The cylindrical Nd:YAG crystal (6x76mm) was embedded inside a flashlamp chamber coupled with a flashlamp (FL). The crystal was surrounded by a Ce, Sm-doped quartz flow tube. The Sm and Ce dopant blocks 1064 nm preventing ASE/parasitics and also blocks some unnecessary pump bands in the visible and UV spectrum. The temperature of the flashlamp chamber was kept constant at room temperature by passing distilled water through the chamber. The flashlamp was controlled by using Analog Modules 8800V flashlamp driver and a home-made trigger circuit. The Nd:YAG crystal was pumped by flashlamp pulses with 150-μs pulsewidth at 1 Hz. The Cr^{4+}:YAG crystal was positioned at Brewster angle to minimize the reflection losses from the surfaces.

The Cr^{4+}:YAG crystal had a dual function inside the optical resonator, a saturable absorber and a Brewster plate to obtain polarized laser output. The Q switching operation was attempted by using two different Cr^{4+}:YAG samples with 91 % and 51 % of small-signal single-pass transmission at 1064nm. When Cr^{4+}:YAG sample with 91 %

transmission was used as the saturable absorber, multiple q-switched pulses were obtained during a single pump pulse because after the first output pulse, the net gain was not depleted completely in a single pump pulse duration. In order to obtain a single pulse, the Cr^{4+}:YAG sample with 51 % of small-signal single-pass transmission was used as the passive optical switch. The temporal trace of the obtained Q-switched pulse is shown in Figure 5.7 for 7 J of pump pulse energy. The pulse was detected by using a Si PIN detector and a 250 MHz digital sampling oscilloscope.

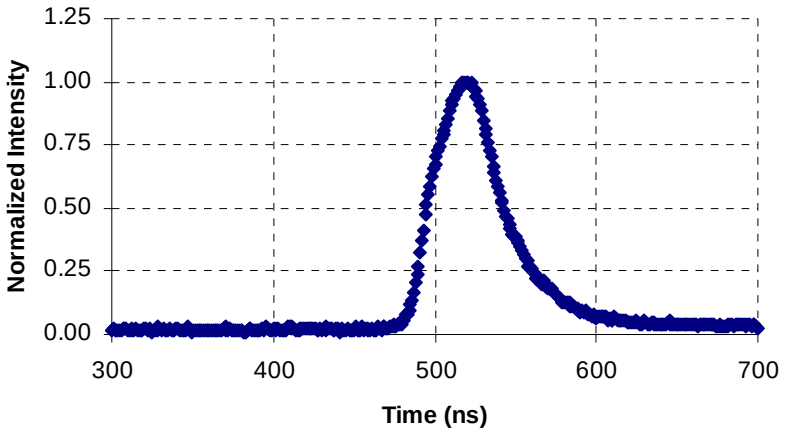

Figure 5.7: The temporal trace of a Q-switched pulse when the pump pulse energy was 7 J. The pulse width was 46.5 ns.

The efficiency measurement of the passively Q-switched Nd:YAG could not be completed because the Cr^{4+}:YAG crystal was damaged during the measurements. When the input pump energy was 17.1 J, the laser photon intensity on the Cr^{4+}:YAG was above the damage threshold of the crystal (Damage threshold > 4 J/cm^2). Figure 5.8 shows the energy efficiency curve take up to an input pump energy of 14.1 J.. As can be seen from Figure 5.8, as high as 83 mJ of output pulse energy was obtained which corresponds to a peak power of 1.8 MW.

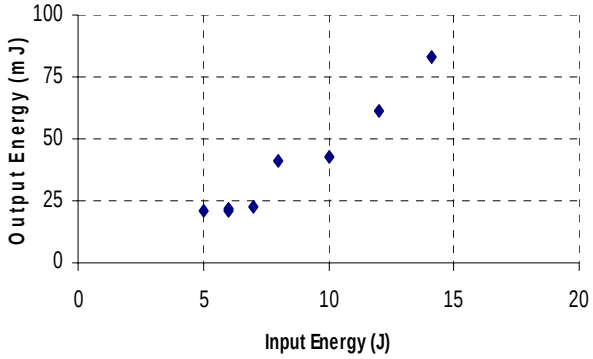

Figure 5.8: Energy efficiency curve for the flashlamp-pumped, passively Q-switched Nd:YAG laser.

Chapter 6

CONCLUSIONS

In this thesis, we first summarized the previously reported studies on the determination of the saturation parameters of Cr^{2+}:ZnSe and Cr^{4+}:YAG saturable absorbers and their applications in passive Q switching. Then, we described the theoretical background needed for the analysis of the saturable absorbers and passive Q switching of solid-state lasers. We experimentally determined the ground-state absorption cross section of Cr^{2+}:ZnSe at the wavelengths of 1800 and 1570 nm to be 6.17×10^{-19} cm^2 and 2.24×10^{-19} cm^2, respectively, and we compared the obtained values with each other by using absorption measurements. We also compared the results with the previously reported values in the literature. In determination of saturation parameters, we used two different experimental techniques and we analyzed the experimental results by using an iterative best-fit algorithm. We also observed that the excited-state absorption in Cr^{2+}:ZnSe was negligible. As an application of the saturable absorbers, we constructed passively Q-switched Nd:YVO_4 and Nd:YAG lasers operating at the wavelength of 1064 nm. Q switching operation was achieved by using the Cr^{4+}:YAG saturable absorbers inside the laser cavity. In the particular case of the Nd:YVO_4 laser, an intracavity lens was used to develop a scheme for adjusting and controlling the pulse repetition rate application. The repetition rate could be varied in the range between 25 and 18 kHz. When the intracavity lens was 9.5 cm away from the output coupler (d_f=9.5 cm), as high as 225 mW of average output power was obtained which corresponds to a peak power of 360 W and a pulse energy of 16.3 μJ. The repetition rate of the Q-switched Nd:YVO_4 laser pulses was measured as a function of the intracavity lens

position and the emission cross section of the Nd:YVO_4 crystal was determined to be $7.7x10^{-19}$ cm^2 from the analysis of the repetition rate measurement. The pulse width remained below 100 ns in this range of the lens position values. In the case of the Nd:YAG laser, as high as 83 mJ of output pulse energy was obtained which corresponds to the peak power of 1.8 MW. The output pulsewidth was 46.5 ns. Higher output energies could not be obtained because the Cr^{4+}:YAG crystal was damaged during the measurements.

BIBLIOGRAPHY

[1] R. H. Page, K. I. Schaffers, L. D. DeLoach, G. D. Wilke, F. D. Patel, J. B. TassanoJr., S. A. Payne, W. F. Krupke, K.-T. Chen, and A. Burger, "Cr^{2+} Doped Zinc Chalcogenides as Efficient, Widely Tunable Mid-Infrared Lasers," *IEEE Journal of Quantum Electronics*, vol. 33, pp. 609-619, 1997.

[2] U. Demirbas, A. Sennaroglu, and M. Somer, "Sythesis and characterization of diffusion-doped Cr^{2+}:ZnSe and Fe^{2+}:ZnSe," *Optical Materials*, vol. 28, pp. 231-240, 2006.

[3] A. Sennaroglu, C. R. Pollock, and H. Nathel, "Efficient continuous-wave chromium-doped YAG laser," *Journal of Optical Society of America B*, vol. 12, pp. 930-937, 1995.

[4] A. Suda, A. Kadoi, K. Nagasaka, H. Tashiro, and K. Midorikawa, "Absorption and oscillation characteristics of a pulsed Cr^{4+}:YAG laser investigated by a double-pulse pumping technique," *IEEE Journal of Quantum Electronics*, vol. 35, pp. 1548-1553, 1999.

[5] H. Eilers, K. R. Hoffman, W. M. Dennis, S. M. Jacobsen, and W. M. Yen, "Saturation of 1.064 um absorption in Cr,Ca:$Y_3Al_5O_{12}$ crystals," *Applied Physics Letters*, vol. 61, pp. 2958-2960, 1992.

[6] A. G. Okhrimchuk and A. V. Shestakov, "Absorption saturation mechanism for YAG:Cr^{4+} crystals," *physical Review B*, vol. 61, pp. 988-995, 2000.

[7] Z. Burshtein, P. Blau, Y. Kalisky, Y. Shimony, and M. R. Kokta, "Excited-state absorption studies of Cr^{4+} Ions in several garnet host crystals," *IEEE Journal of Quantum Electronics*, vol. 34, pp. 292-299, 1998.

[8] G. Xiao, J. H. Lim, S. Yang, E. V. Stryland, M. Bass, and L. Weichman, "Z-scan measurement of the ground and excited state absorption cross sections of Cr^{4+} in Yttrium aluminum garnet," *IEEE Journal of Quantum Electronics*, vol. 35, pp. 1086-1091, 1999.

[9] A. Sennaroglu, "Continuous-wave thermal loading in saturable absorbers: theory and experiment," *Applied Optics*, vol. 36, pp. 9528-9535, 1997.

[10] Y. Kalisky, A. B.-A. Baranga, Y. Shimony, and M. R. Kokta, "Cr $^{4+}$ doped garnets: novel laser materials and non-linear saturable absorbers," *Optical Materials*, vol. 8, pp. 129-134, 1997.

[11] K. Spariosu, W. Chen, R. Stultz, and M. Birnbaum, "Dual Q Switching and laser action at 1.06 and 1.44 um in a Nd^{3+}:YAG-Cr^{4+}:YAG oscillator at 300 K," *Optics Letters*, vol. 18, pp. 814-816, 1993.

[12] A. Sennaroglu, U. Demirbas, S. Ozharar, and F. Yaman, "Accurate determination of saturation parameters for Cr^{4+}-doped solid-state saturable absorbers," *Journal of Optical Society of America B*, vol. 23, pp. 241, 2006.

[13] N. N. Ilichev, A. V. Kiryanov, E. S. Gulyamova, and P. P. Pashinin, "Influence of the nonlinear anisotropy of absorption in a passive Cr4+:YAG switch on the energy and polarisation characteristics of a neodymium laser," *Quantum Electronics*, vol. 27, pp. 298-301, 1997.

[14] I. J. Miller, A. J. Alcock, and J. E. Bernard, "Experimental Investigation of Cr^{4+} in YAG as a Passive Q-Switching," presented at OSA Proceedings on Advanced Solid-State Lasers, 1992.

[15] P. Yankov, "Cr^{4+}:YAG Q-switching of Nd: host laser oscillators," *J. Phys. D: Appl. Phys.*, vol. 27, pp. 1118-1120, 1994.

[16] Y. Shimony, Z. Burshtein, and Y. Kalisky, "Cr^{4+}:YAG as passive Q-switch and Brewster plate in a pulsed Nd:YAG laser," *IEEE Journal of Quantum Electronics*, vol. 31, pp. 1738-1741, 1995.

[17] Y. Shimony, Y. Kalisky, and B. H. T. Chai, "Quantitative studies of Cr^{4+}:YAG saturable absorber for Nd:YAG laser," *Optical Materials*, vol. 4, pp. 547-551, 1995.

[18] Y. Shimony, Z. Burshtein, A. B.-A. Baranga, Y. Kalisky, and M. Strauss, "Repetitive q-switching of a CW Nd:YAG laser using Cr^{4+}:YAG saturable absorbers," *IEEE Journal of Quantum Electronics*, vol. 32, pp. 305-310, 1996.

[19] H. T. Powell and G. J. Wolga, "Repetitive Passive Q-switching of Single-Frequency Lasers," *IEEE J. Quantum Electron.*, vol. QE-1, pp. 213-219, 1971.

[20] K. Waichman and Y. Kalisky, "Repetitive modulation and passively Q-switched CW diode pumped Nd-doped lasers," *Optical Materials*, vol. 19, pp. 149-159, 2002.

[21] J. Liu, J. Yang, and J. He, "High repetition rate passively Q-switched diode-pumped Nd:YVO_4 laser," *Optics & Laser Technology*, vol. 35, pp. 431-434, 2003.

[22] A. Agnesi and S. Dell'acqua, "High-peak-power diode-pumped passively Q-switched Nd:YVO_4 laser," *Applied Physics B*, vol. 76, pp. 351-355, 2003.

[23] T.-Y. Tsai and M. Birnbaum, "Q -Switched 2- μm lasers by use of a Cr^{2+}:ZnSe saturable absorber," *Applied Optics*, vol. 40, pp. 6633-6637, 2001.

[24] A. V. Podlipensky, V. G. Shcherbitsky, N. V. Kuleshov, and V. P. Mikhailov, "Cr^{2+}:ZnSe and Co^{2+}:ZnSe saturable-absorber Q switches for 1.54-μm Er:glass lasers," *Optics Letters*, vol. 24, pp. 960-962, 1999.

[25] F. Z. Qamar and T. A. King, "Passive q-switching of Tm-silica fibre laser near 2 μm by a Cr^{2+}:ZnSe saturable absorber crystal," *Optics Communications*, vol. 248, pp. 501-508, 2005.

[26] R. D. Stultz, V. Leyva, and K. Spariosu, "Short pulse, high-repetition rate, passively q-switched Er:yttrium-aluminum-garnet laser at 1.6 microns," *Applied Physics Letters*, vol. 87, pp. 241118, 2005.

[27] J. T. Vallin, G. A. Slack, S. Roberts, and A. E. Hughes, "Infrared Absorption in Some II-VI Compounds Doped with Cr," *Physical Review B*, vol. 2, pp. 4313-4333, 1970.

[28] A. V. Podlipensky, Shcherbitsky, V.G., Kuleshov, N.V., Mikhailov, V.P., "Cr^{2+}:ZnSe and Co^{2+}:ZnSe saturable-absorber Q switches for 1.54-μm Er:glass lasers," *Optics Letters*, vol. 24, pp. 960-962, 1999.

[29] V. G. Shcherbitsky, S. Girard, M. Fromager, R. Moncorge, N. V. Kuleshov, V. I. Levchenko, V. N. Yakimovich, and B. Ferrand, "Accurate method of the measurement of absorptioncross sections of solid-state saturable absorbers," *Applied Physics B*, vol. 74, pp. 367-374, 2002.

[30] I. T. Sorokina, "Crystalline Mid-Infrared Lasers," in *Solid-State Mid-Infrared Laser Sources*, vol. 89, *Springer Topics in Applied Physics*, I. T. Sorokina and K. L. Vodopyanov, Eds. Berlin Heidelberg: Springer, 2003, pp. 255-349.

[31] Y.-K. Kuo, M.-F. Huang, and M. Birnbaum, "Tunable Cr^{4+}:YSO Q-switched Cr:LiCAF laser," *IEEE Journal of Quantum Electronics*, vol. 31, pp. 657-663, 1995.

[32] V. E. Kisel, V. G. Shcherbitsky, N. V. Kuleshov, V. I. Konstantinov, V. I. Levchenko, E. Sorokin, and I. Sorokina, "Spectral kinetic properties and lasing characteristics of diode-pumped Cr2+: ZnSe single crystals," *Optics and Spectroscopy*, vol. 99, pp. 663-667, 2005.

[33] G. J. Spühler, R. Paschotta, R. Fluck, B. Braun, M. Moser, G. Zhang, E. Gini, and U. Keller, "Experimentally confirmed design guidelines for passively Q-switched microchip lasers using semiconductor saturable absorbers," *Journal of Optical Society of America*, vol. 16, pp. 376-388, 1999.

[34] A. V. Podlipensky, V. G. Shcherbitsky, N. V. Kuleshov, V. I. Levchenko, V. N. Yakimovich, M. Mond, E. Heumann, G. Huber, H. Kretschmann, and S. Kück, "Efficient laser operation and continuous-wave didode pumping of Cr^{2+}:ZnSe single crystals," *Applied Physics B*, pp. 253-255, 2001.

[35] A. Sennaroglu, A. Kurt, and S. Buhours, "Analysis and optimization of diode end-pumped solid-state lasers: Application to Nd3+:YVO4 Lasers at 1064 and 1342 nm," *Optical Engineering*, vol. 44, pp. 054202, 2005.